

Review

# Recent Advances in Metal-Based Molecular Photosensitizers for Artificial Photosynthesis

Lei Wang 

School of Materials and Chemistry, University of Shanghai for Science and Technology, Shanghai 200093, China; leiwang@usst.edu.cn

**Abstract:** Artificial photosynthesis (AP) has been extensively applied in energy conversion and environment pollutants treatment. Considering the urgent demand for clean energy for human society, many researchers have endeavored to develop materials for AP. Among the materials for AP, photosensitizers play a critical role in light absorption and charge separation. Due to the fact of their excellent tunability and performance, metal-based complexes stand out from many photocatalysis photosensitizers. In this review, the evaluation parameters for photosensitizers are first summarized and then the recent developments in molecular photosensitizers based on transition metal complexes are presented. The photosensitizers in this review are divided into two categories: noble-metal-based and noble-metal-free complexes. The subcategories for each type of photosensitizer in this review are organized by element, focusing first on ruthenium, iridium, and rhenium and then on manganese, iron, and copper. Various examples of recently developed photosensitizers are also presented.

**Keywords:** molecular photosensitizers; catalysis; metal complexes; artificial photosynthesis



**Citation:** Wang, L. Recent Advances in Metal-Based Molecular Photosensitizers for Artificial Photosynthesis. *Catalysts* **2022**, *12*, 919. <https://doi.org/10.3390/catal12080919>

Academic Editor: Bishweshwar Pant

Received: 26 July 2022

Accepted: 17 August 2022

Published: 19 August 2022

**Publisher's Note:** MDPI stays neutral with regard to jurisdictional claims in published maps and institutional affiliations.



**Copyright:** © 2022 by the author. Licensee MDPI, Basel, Switzerland. This article is an open access article distributed under the terms and conditions of the Creative Commons Attribution (CC BY) license (<https://creativecommons.org/licenses/by/4.0/>).

## 1. Introduction

Over the past several decades, a large amount of fossil fuels have been exploited, especially during the Industrial Revolution [1–3]. The overexploitation of fossil fuels not only destroys the environment but has also led to serious global climate change and an energy crisis, which directly threaten the survival of humanity. To resolve these problems, thousands of green power sources are in development [4–6]. The Sun provides much more energy than current global demand; hence, it has become desirable in the development of novel sustainable energy. Artificial photosynthesis (AP), such as photocatalytic water splitting or CO<sub>2</sub> reduction, can achieve the conversion of solar energy into chemical fuels, including carbon-free hydrogen as an environmentally friendly fuel, and industrial raw materials such as methanol [7–10]. Among various photosynthetic systems, molecular-based multi-component systems have been a research hotspot because of their properties, which can be controlled by the reasonable design of their chemical structures [11–13]. In a multi-component system, a photosensitizer plays an important role in light absorption and electron transfer; therefore, intense research has been devoted to photosensitizers, particularly from 2012 to 2022 as shown in Figure 1. This booming exploration of metal-complex-based photosensitizers has resulted in improving their performance and availability for commercial applications.

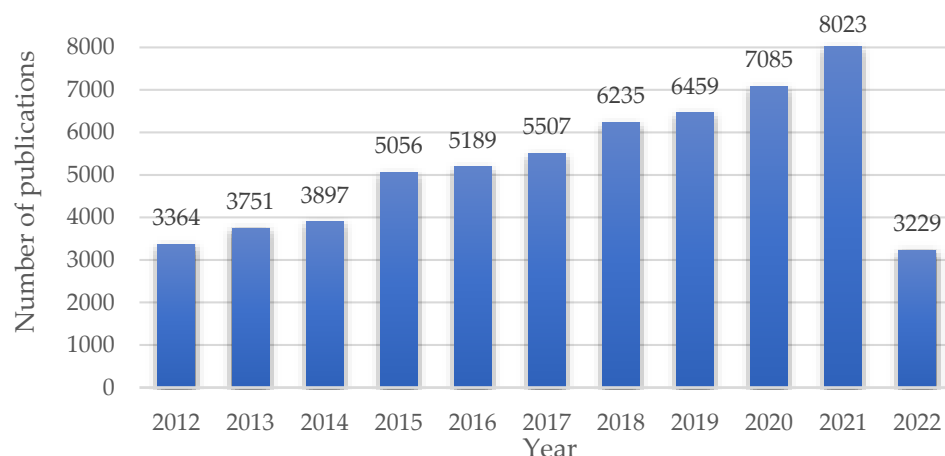


**Figure 1.** Number of publications concerning “photosensitizer” subjects since 2012. Adapted from ISI Web of Science, dated 12 July 2022.

### 1.1. Photosynthesis in Nature

Natural photosynthesis in green plants and cyanobacteria is a critical reaction for the utilization of sunlight, which is crucial for providing sustainable energy on Earth. Photosynthesis in nature occurs through two unique photosystems, i.e., PSI and PSII, involving several electron transfer (ET) procedures [14]. As shown in Figure 2a, PSII is triggered by the photoexcitation of P680 and the release of electrons to give P680<sup>+</sup>, which is then involved in an oxygen-evolving reaction (OER). Simultaneously, PSI is initiated by the photoexcitation of P700, which then accepts electrons from the ET chain of PSII, resulting in the activation of the Calvin cycle, where CO<sub>2</sub> is reduced into carbohydrates.

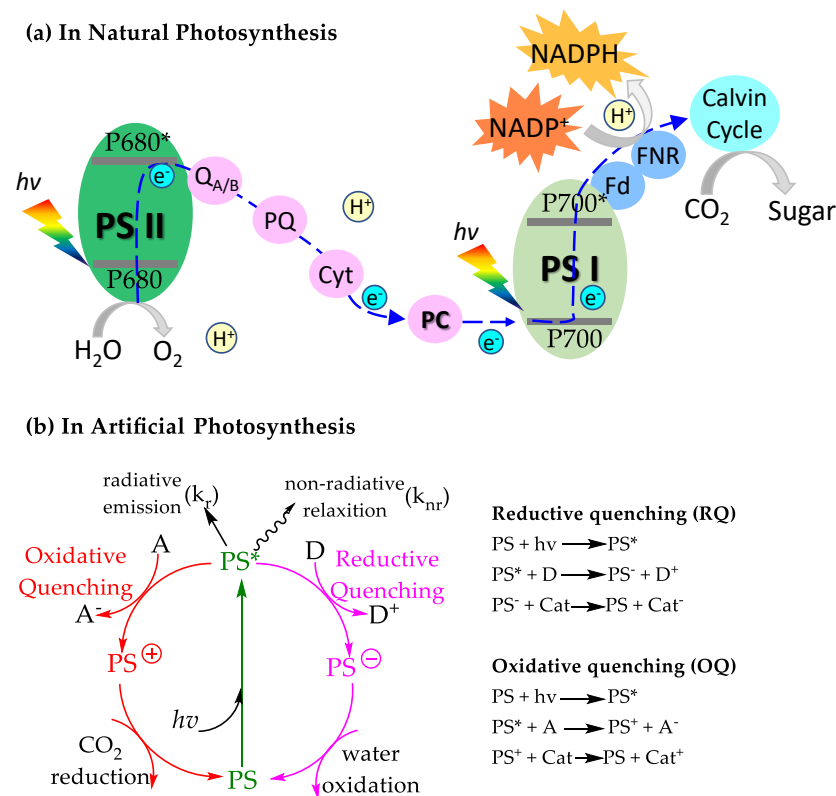


**Figure 2.** (a) The Z-scheme coupling PSI and PSII in natural photosynthesis; (b) the general scheme of the quenching pathway in photocatalytic reactions. PS: photosensitizer; A: electron acceptor; D: electron donor; Cat: catalyst. \*: excited state.

### 1.2. The Role of Photosensitizers in Artificial Photosynthesis

Inspired by nature, artificial photosynthesis (AP) simulates the function of critical components in a photocatalytic reaction [15]. Unlike natural photosynthesis, AP can not only convert CO<sub>2</sub> into biomass, but it can also produce various chemical fuels such as hydrogen. There are three processes in a multi-component artificial photosynthesis reaction: (i) the light harvesting process in which a photosensitizer absorbs sunlight efficiently and then is converted into an excited state (PS\*); (ii) the charge generation and separation step in which electron-transfer occurs between the PS\* and an e<sup>-</sup> acceptor/donor; (iii) a catalytic reaction. Clearly, a photosensitizer plays an important role in the absorption of solar photons and the injection of the photoexcited electrons into an acceptor in a photocatalytic reaction.

### 1.3. A General Scheme for Photosensitizer-Involved Photocatalysis

Figure 2b illustrates a general scheme for a photosensitizer-involved AP reaction. A ground-state photosensitizer (PS) is excited by sunlight and form PS\* via a metal-to-ligand charge transfer (MLCT), i.e., electron-transfer occurs between the metal orbital and ligand orbital. PS\* then undergoes electron transfer quenching (reductive or oxidative) in the presence of a donor or an acceptor, i.e., sacrificial agent (SA) resulting in the formation of a reduced photosensitizer (PS<sup>-</sup>) or oxidized photosensitizer (PS<sup>+</sup>). Finally, PS<sup>-</sup> or PS<sup>+</sup> can be re-oxidized or be re-reduced back to PS in a catalytic reaction for CO<sub>2</sub> reduction, hydrogen generation, or water oxidation [16–18]. However, it is worth noting that there are two competing side reactions that take place: (i) the PS\* decays to PS by heat or a nonradiative pathway; (ii) back electron transfer occurs between SA<sup>-</sup> and PS<sup>+</sup> or between SA<sup>+</sup> and PS<sup>-</sup>. Therefore, to improve the overall photocatalytic efficiency, the lifetime of an excited state PS\* must be long enough to overcome these side reactions. Meanwhile, it requires that PS<sup>-</sup> or PS<sup>+</sup> provides a suitable driving force to make catalysis occurs. In addition, because solar irradiation (AM1.5G) consists of only ~4% ultraviolet light ( $\lambda < 400$  nm) and ~43% near-infrared light ( $\lambda > 800$  nm) but also ~53% visible light ( $400 \text{ nm} < \lambda < 800$  nm), the ground-state PS should absorb as much visible light as possible to obtain a strong amount of energy from sunlight [19].

Due to the crucial role of photosensitizer(s) in AP, a comprehensive review on photosensitizers for solar hydrogen generation was published in 2017 [20]. In this review, some criteria of evaluating molecular photosensitizers were first described, and then recent achievements on metal-based photosensitizers and their importance in artificial photosynthesis were summarized and highlighted. The photosensitizers were categorized into two main families: noble-metal and noble-metal-free complexes. Noble-metal photosensitizers include ruthenium-, iridium-, and rhenium-based complexes, while noble-metal-free photosensitizers contain manganese-, iron-, copper-, and other metal-based complexes.

## 2. Parameters for Evaluating Photosensitizers

Some desirable characteristics for a photosensitizer include: (i) strong absorption of a distinguished range of the solar spectrum; (ii) a long excited-state lifetime (ns~ $\mu$ s); (iii) chemical stability in solution; (iv) reversible redox potentials. Therefore, several parameters are derived to evaluate the performance of photosensitizers.

### 2.1. UV-Vis Absorption

In metal coordinating complexes, intense absorptions may arise from the transfer of electronic charges between ligand orbitals and metal orbitals, either ligand-to-metal charge transfer (LMCT) or metal-to-ligand charge transfer (MLCT). Since ligands for MLCT usually have vacant, low-lying  $\pi^*$  orbitals, such as py, bpy, phen, and other aromatic ligands, which are widely used in molecular metal photosensitizers, MLCT has been discussed in previous studies more often than LMCT in photocatalytic processes; hence, herein, MLCT was the focus. As mentioned previously, charge transfer transition is a critical process in artificial photosynthesis. For effective utilization of solar light, a basic requirement

for a photosensitizer is absorbing sunlight over the visible wavelength and initiating electron transfer *from* or *to* its excited state. Using the description above, measuring UV-Vis absorption is usually the first and one of the most important steps in estimating the photocatalytic applications of a photosensitizer.

There are two main parameters that can be obtained by the UV-Vis spectrum:

(i) The charge transfer wavelength  $\lambda$  (in nm):

$$E_{\text{MLCT}} \left( \text{cm}^{-1} \right) = \frac{10^7}{\lambda \text{ (nm)}} \quad (1)$$

$$E_{\text{MLCT}} \text{ (eV)} = \frac{E_{\text{MLCT}} \left( \text{cm}^{-1} \right)}{8065} \quad (2)$$

(ii) The molar extinction coefficient (or absorption), which is independent of concentration, and calculated by:

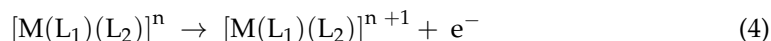
$$\varepsilon = \frac{A_{\text{max}}}{cl} \left( \text{dm}^3 \text{ mol}^{-1} \text{ cm}^{-1} \right) \quad (3)$$

where  $A_{\text{max}}$  is the maximum absorbance;  $c$  is measured in  $\text{mol dm}^{-3}$ , and the cell path length,  $l$ , is in cm.

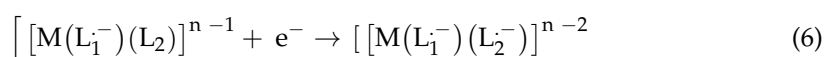
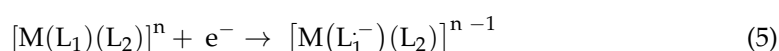
## 2.2. Ground-State Redox Potential

The ground-state redox properties of photosensitizers are important indicators for photocatalysis. A common method of measuring ground-state redox potentials for metal complexes is cyclic voltammetry (CV). Generally, CV can reflect the oxidation of the metal center and the reduction of ligands in a complex. Take the  $[\text{M}(\text{L}_1)(\text{L}_2)]^n$  complex, owing to its MLCT character, as an example [21]. The electron transfer processes are:

(i) Oxidation:



(ii) Reductions:



In addition to the oxidation and reduction abilities, the stability of a photosensitizer is another important consideration, since it must be capable of being regenerated over multiple turnovers in a photosynthesis reaction. As a result, the reversibility of the above redox processes, being demonstrated by cyclic voltammetry, is also important.

Since MLCT transition is accompanied by the occurrence of metal oxidation and ligand reduction, a correlation between the energies of the charge transfer absorptions and the electrochemical properties is established without considering the solvation and electron correlation effects:

$$E_{\text{MLCT}} = \left| E(\text{M}^{n+1}/\text{M}^n) \right| + \left| E(\text{L}^-/\text{L}) \right| \quad (7)$$

Evidently, the electrochemical data deconvolve important details, but the value of  $E_{\text{MLCT}}$  alone is insufficient to determine whether a photosensitizer is suitable for a photocatalysis reaction.

## 2.3. Steady-State Emission

For a typical metal-based photosensitizer, the radiative quantum yield ( $\Phi$ ) can be calculated from the ratio between the number of emitted photons and the number of absorbed photons:

$$\phi = \frac{I_{\text{em}}}{I_{\text{abs}}} \quad (8)$$

where  $I_{em}$  can be obtained from the steady-state emission spectrum.

According to Lakowicz's method in *Principles of Fluorescence Spectroscopy* [22], the relative quantum yield can be calculated using Equation (9):

$$\Phi_p = \Phi_{ref} \times \frac{Int_p}{Int_{ref}} \times \frac{(1 - 10^{-A_{ref}})}{(1 - 10^{-A_p})} \times \frac{\eta_p^2}{\eta_{ref}^2} \quad (9)$$

where  $Int$  is the area under the emission peak;  $A$  is the absorbance at the excitation wavelength;  $\eta$  is the refractive index of the solvent. For the same type of photosensitizers in the same solvent, the absorbance value  $A$  is similar and  $\eta$  is the same, and the above equation can be simplified as Equation (10):

$$\Phi_p = \Phi_{ref} \times \frac{Int_p}{Int_{ref}} \quad (10)$$

#### 2.4. Excited-State Redox Potential

For a multi-component photocatalytic process, the driving force of a photosensitizer must be adequate. As a result, the value of  $E([M]^{n+1}/[M]^n)$ , which reflects the electron-donating ability, must be more negative than the reduction potential of the catalyst so that electron(s) can be transferred *from* the excited state to the catalyst. Conversely, the value of  $E([M]^n/[M]^{n-1})$ , which reflects the electron-accepting ability, must be more positive than the reduction potential of the catalyst (usually in a high oxidation state) to ensure the electron transfer occurs to the excited state. In this way, the excited-state redox potentials for molecular photosensitizers are calculated by the following equations:

(i) Oxidative quenching:

$$E([M]^{n+1}/[M]^{n*}) = E([M]^{n+1}/[M]^n) - E_0 \quad (11)$$

$$E(L^*/L^-) = E(L^0/L^-) + E_0 \quad (12)$$

(ii) Reductive quenching:

$$E([M]^n/[M]^{(n-1)*}) = E([M]^n/[M]^{n-1}) + E_0 \quad (13)$$

$$E(L^-/L^*) = E(L^-/L) - E_0 \quad (14)$$

where  $E([M]^{n+1}/[M]^n)$  and  $E([M]^n/[M]^{n-1})$  are the ground-state potentials.  $E_0$  can be estimated from one of the following methods: (i) the crossover point of the lowest-energy MLCT absorption band and the corresponding emission band [23]; (ii) the crossover point of the tangent line of the emission spectrum (left half) with a wavelength axis [24]; (iii) the first vibronic band in the low-temperature emission spectrum [25] (see details below).

Clearly, the excited-state redox potential is an important indicator for evaluating photosensitizers, but it should be noted that the calculation of the excited-state redox potential may have some error because of the uncertainty of  $E_0$ .

#### 2.5. Lifetime

To simplify our discussion, two states for a photosensitizer after being excited are shown in Figure 3: the singlet state <sup>1</sup>MLCT ( $S_1$ ) and the triplet state <sup>3</sup>MLCT ( $T_1$ ). The  $S_1$  state can decay to the ground state ( $S_0$ ) via a radiative way, i.e., fluorescence ( $k_r$ ) and/or a nonradiative way ( $k_{nr}$ ). Afterwards, the singlet-triplet transition happens through intersystem crossing (ISC) with the association of energy loss as heat ( $k_{ISC}$ ). Thereafter, the  $T_1$  state's decay to the  $S_0$  state follows a similar way as the  $S_1$  state: a radiative way, i.e., phosphorescence ( $k'_r$ ) and/or a nonradiative way ( $k'_{nr}$ ). Therefore, these decay constants (hence, lifetime) are important criteria for evaluating a photosensitizer.

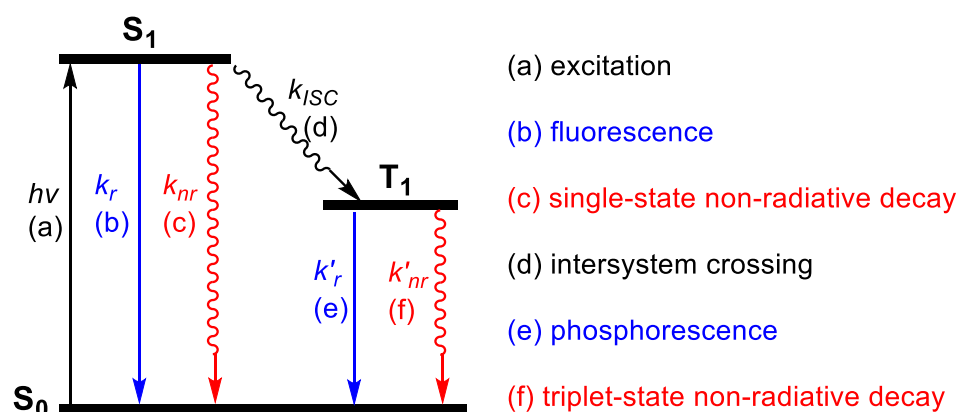


**Figure 3.** Jablonski diagram of a typical metal-based photosensitizer. Adapted with permission from ACS Energy Lett. 2019, 4, 2, 558–566. Copyright 2019 American Chemical Society.

Generally, the lifetime ( $\tau_0$ ) of a photosensitizer is measured by excited-state transient absorption (TA) spectra and the signal fit to single [24] or triple [26] (depends on the mechanism of photosensitizers) exponential decay kinetics. To complete a photocatalytic reaction, the excited-state lifetime must be long enough to overcome the decay process.

$$\tau_0 = \frac{1}{k_r + k_{nr}} \quad (15)$$

where  $k_r = \phi_0 \times k_0$ ;  $k_{nr} = (1 - \phi_0) \times k_0$ .

Through measuring  $\tau_0$ ,  $k_r$  can be calculated by Equation (16):

$$k_r = \frac{\phi_p}{\tau_0} \quad (16)$$

Therefore,  $k_{nr}$  can be calculated by combining Equations (9), (15) and (16) as shown below:

$$k_{nr} = \frac{1 - \phi_p}{\tau_0} \quad (17)$$

### 2.6. Marcus Electron-Transfer Theory

Since photocatalytic reactions are essentially electron transfer (ET) processes, the kinetics of ET is governed by Marcus theory, shown in Equation (18).

$$k_{ET} = \left( \frac{k_B T}{h} \right) \exp \left[ \frac{-(\lambda + \Delta G_0)^2}{4\lambda k_B T} \right] \quad (18)$$

where  $k_B$  refers to the Boltzmann constant;  $T$  is the temperature (K);  $h$  refers to Planck's constant;  $\lambda$  refers to the reorganization energy.  $\Delta G_0$  is the driving force of the electron-transfer reaction as shown below:

$$\Delta G_0 = E_h (\text{electron donor}) - E_h (\text{electron acceptor}) \quad (19)$$

Apparently, increasing the driving force can improve the rate of electron transfer, i.e., the rate of catalysis as indicated by the excited-state potential equations and the Marcus relationship [27]. However, Marcus theory also demonstrates that there is a Marcus inverted region, where a stronger driving force leads to slower ET rates, hence, there is no normal standard criterion for photosensitizers for all photocatalytic reactions.

### 2.7. Stern-Volmer Quenching

Because of the occurrence of back-electron transfer between photosensitizers and catalysts, it is necessary to add a sacrificial reagent to most photocatalytic reactions.  $K_{SV}$  is calculated from the emission quenching data as a function of the concentration of persulfate, which follows the Stern–Volmer relationship:

$$\frac{I_0}{I} = k_{sv} [S_2O_8^{2-}] + 1 \quad (20)$$

where

$$k_{sv} = \tau_0 \times k_q \quad (21)$$

Using above discussions, the radiative quantum yield of a photosensitizer shows a dependent relationship with the concentration of a quencher, i.e., [Q]:

$$\phi_q = \frac{k_r}{k_0 + k_q[Q]} \quad (22)$$

$$\frac{\phi_0}{\phi_q} = 1 + \frac{k_q[Q]}{k_0} \quad (23)$$

### 2.8. Turnover Frequency (TOF)

TOF is an essential parameter of a catalyst, reflecting its catalytic activity and performance. A recent review by Xiujuan Wu and Licheng Sun outlined several calculation methods for evaluating catalysts [28]. It is less common to calculate the TOF for a photosensitizer than for a catalyst but, in some cases, when a standard catalyst is applied, TOF becomes an important criterion for comparing the performances of different photosensitizers. From the perspective of a definition, TOF refers to the amount of product converted from the reactant per mol of the effective photosensitizer per unit time.

$$TON = \frac{\text{amount of transferred electrons for product (moles)}}{\text{amount of photosensitizer (moles)}} \quad (24)$$

$$TOF = \frac{TON}{\text{time of reaction}} \quad (25)$$

Since the plot of TON versus time does not usually follow a linear relationship, the TOF is taken from the pseudo-first-order rate constant, i.e., the maximum photocatalytic rate.

## 3. Noble-Metal-Based Photosensitizers

Noble metals, such as Ru [29], Ir [30], Pt [31–34], Os [35,36], and Re [37], have been extensively investigated as photosensitizers for artificial photosynthesis. These complexes have received wide attention due to the fact of their attractive photophysical electrochemical properties such as visible-light <sup>1</sup>MLCT, long excited-state lifetime, high photocatalytic driving force, and high catalytic activities.

### 3.1. Ru-Based Photosensitizers

The ruthenium-polypyridine family is an early-developed photosensitizer [38], and its fundamental properties and mechanisms have been well investigated [39–43]. Current research efforts on this family of photosensitizer focus on improving its photochemical stability, antidecomposition, extreme pH value tolerance, and driving force at various environmental conditions.

Concepcion et al. developed a series of homoleptic Ru(II) polypyridyl complexes (Figure 4a), which showed decent photochemical water oxidation performance at pH 1 [24]. By modifying electron-withdrawing groups (i.e.,  $-CF_3$  and  $-PO_3H_2$ ) at the 4, 4', or 5' positions of bpy ligands, the redox potentials increased to as high as 1.6 V (vs. NHE) at pH 1. It is worth mentioning that unlike heteroleptic complexes, the redox potentials of

which can be increased at the expense of decreasing the excited-state lifetimes [44], some of these homoleptic Ru(II) polypyridyl complexes presented increased lifetimes from 580 to 731 ns at pH 1. Their studies illustrated that replacing H with electron-withdrawing groups in homoleptic complexes provides a feasible strategy for designing and synthesizing high-performing photosensitizers at pH 1. The kinetic isotope effects (KIEs) of the PO<sub>3</sub>H<sub>2</sub>-containing complexes proved the concerted EPT between the photosensitizer and catalyst for the first time.

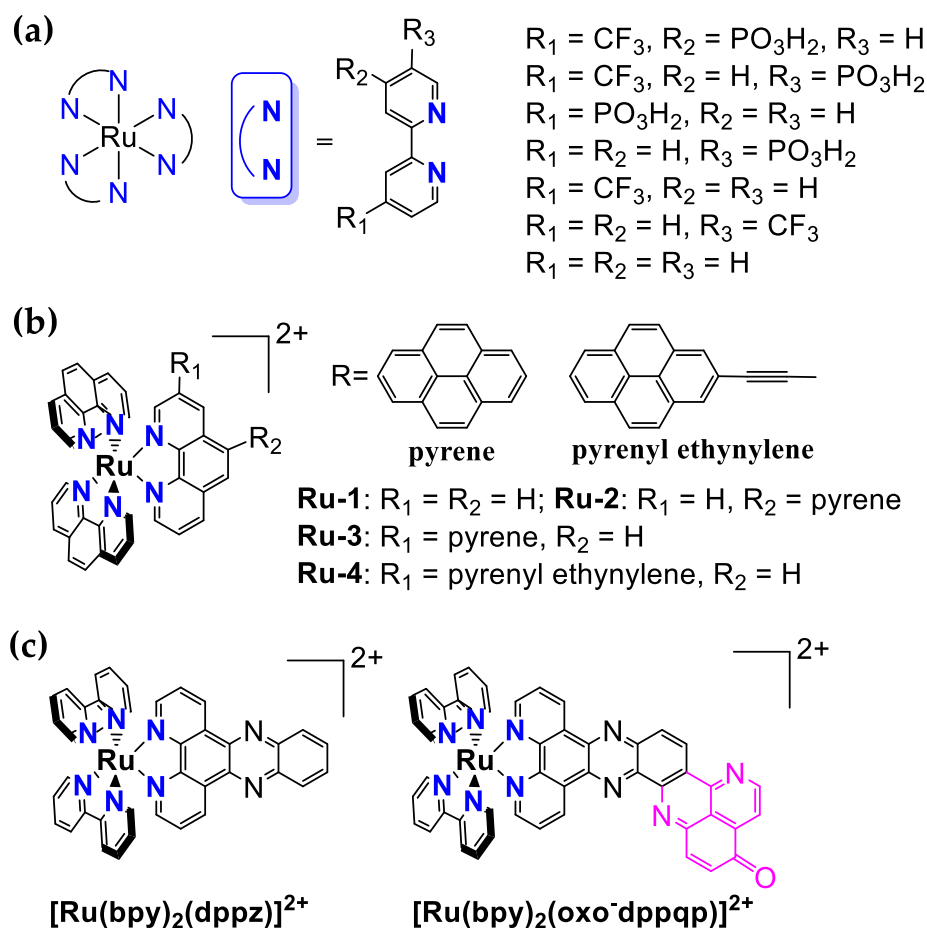


**Figure 4.** Chemical structures of the (a) [Ru(bpy)<sub>3</sub>]<sup>2+</sup>-based, (b) [Ru(phen)<sub>3</sub>]<sup>2+</sup>-based, and (c) [Ru(bpy)<sub>2</sub>(dppz)]<sup>2+</sup>-based photosensitizers and corresponding ligands in this review.

In addition to [Ru(bpy)<sub>3</sub>]<sup>2+</sup>-type photosensitizers, [Ru(phen)<sub>3</sub>]<sup>2+</sup> complexes are another family of Ru photosensitizers, but they are more used in CO<sub>2</sub> reduction reactions (CO<sub>2</sub>RR). However, the excited-state lifetime of raw [Ru(phen)<sub>3</sub>]<sup>2+</sup> complexes is short (360 ns in CH<sub>3</sub>CN), resulting in a weakened photocatalytic performance for CO<sub>2</sub>RR. It has been proved that adding a conjugated group can improve the excited-state lifetime, but an improper introduction will make the excited oxidation potentials worse. To address this problem, Lu et al. creatively synthesized pyrene-modified [Ru(phen)<sub>2</sub>(L)]<sup>2+</sup> photosensitizers (Figure 4b) and realized the fine-tuning of PS properties for efficient CO<sub>2</sub> reduction. The conjugated group, pyrene, greatly improved the sensitizing ability of [Ru(phen)<sub>3</sub>]<sup>2+</sup> complexes. Especially, [Ru(phen)<sub>2</sub>(3-pyrenylphen)]<sup>2+</sup> (**Ru-3**) showed a moderate excited-state lifetime (68.2 μs) but a 17 times larger TOF than [Ru(phen)<sub>3</sub>]<sup>2+</sup> with a large TON of 66,480 [45]. Their study clearly illustrated the importance of balancing lifetime and potential in improving the overall performance of photocatalytic systems.

In recent years, multielectron accumulation has been considered an effective strategy for improving photocatalytic performance. Several studies have shown that naphthalene [46], anthraquinone [47], and dipyrrolo-[3,2-a:2',3'-c]phenazine (dppz) [48] own the

electron-storage ability and can enhance the efficiency of light-driven processes. These bent-bridging-ligands involve ruthenium complexes; however, they usually require ingenious design of molecular structures and smart synthesis procedures for ligands. On the foundation of dppz-based complexes, Dietzek and Kerlidou et al. modified a pyridoquinolinone subunit on dppz (Figure 4c) [49] aimed at realizing electron accumulation by extending the  $\pi$  system. Various methods proved the  $2e^-/2H^+$  mechanism of this photosensitizer and demonstrated its potential applications in producing  $H_2O_2$ .

### 3.2. Ir-Based Photosensitizers

Although Ru-based photosensitizers have shown vast potential in solar energy conversion, their poor photostability limit their application. In responding to this problem, Ir (III) complexes have drawn particular attention in replacing Ru (II) complexes over the past decade. In 2018, Bernhard et al. thoroughly reviewed Ir (III)-type photosensitizers [50]; hence, this review focused only on the development of Ir photosensitizers thereafter.

$[Ir(ppy)_2(bpy)]^+$  and its derivatives (Figure 5a) have been extensively studied as photosensitizers for energy conversion due to the fact of their decent photostability. Based on these studies, in 2020, Dietzek et al. developed and studied a series of iridium complex-polyoxometalate (POM) dyads, Ir-POM<sub>M</sub>, which have shown high efficiency in photocatalytic hydrogen evolution reactions [51,52]. By changing the central metal of POM from  $Mn^{3+}$  to  $Fe^{3+}$  to  $Co^{3+}$ , the yields of charge-separated state  $Ir^+-POM_M^-$  (i.e., the rate-limiting intermediate) decreased, while the lifetime increased from 290 to 540 ps. A photoinduced electron transfer dynamics study illustrated that the catalytic capacity decreased in the order Ir-POM<sub>Mn</sub> > Ir-POM<sub>Co</sub> > Ir-POM<sub>Fe</sub>, which was in the same order of the yields of  $Ir^+-POM_M^-$ , demonstrating the high impact of yield on the catalytic capacity.

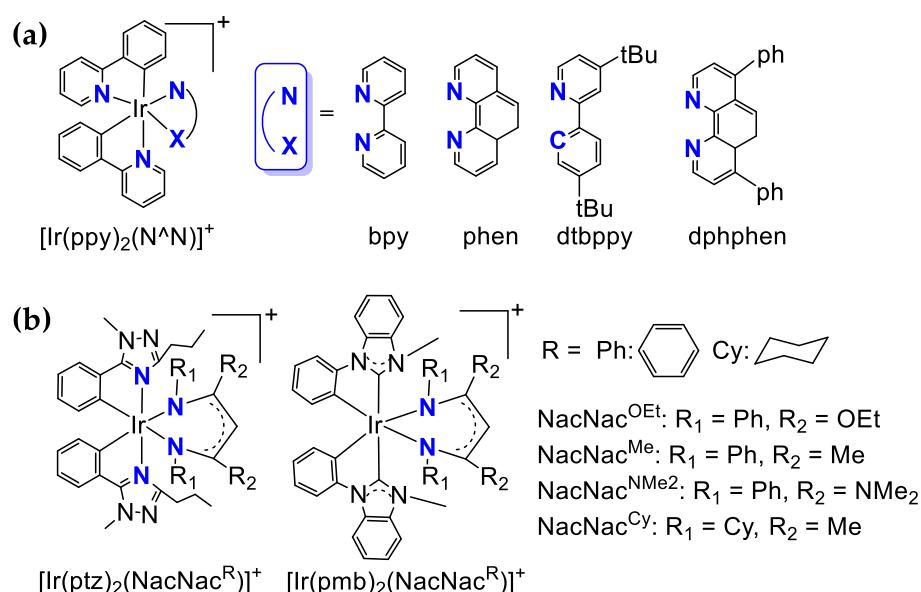


**Figure 5.** Chemical structures of the (a)  $[Ir(ppy)_2(bpy)]^+$ -based and (b)  $\beta$ -diketiminato-modified (NacNac) iridium photosensitizers and corresponding ligands in this review.

In 2021, Teets et al. prepared a series of  $\beta$ -diketiminato-modified (NacNac) iridium complexes as demonstrated in Figure 5b. The electron-rich NacNac ligands dramatically improved the photoinduced electron transfer rate, as indicated by the decreased excited redox potential from  $-2.1$  to  $-2.5$  V (vs.  $Fc^+/Fc$ ), making various challenging photoredox reactions occur under moderate conditions with high yield [53,54]. Later, they further improved the photocatalytic performance by replacing ppy with ptz and pmb, all of which presented significant excited redox potentials in the range of  $-2.4$  to  $-2.8$  V [55]. Their studies put forward practical proposals for designing novel photosensitizers with high efficiency and feasible photostability.

### 3.3. Re-Based Photosensitizers

Rhenium photosensitizers are usually found in the family of  $[\text{Re}(\text{bpy})(\text{CO})_3\text{Cl}]$  complexes. Ishitani et al. developed a series of highly efficient rhenium(I) trinuclear photosensitizers (Figure 6a) for photocatalytic  $\text{CO}_2$  reduction [56]. As a consequence of the efficient reductive quenching of the Re-ring by triethanolamine and fast electron transfer, the  $\text{CO}_2$  reduction process showed high photocatalytic efficiencies. A summary of the characteristics and properties of Re(I) diimine complexes were published by Ishitani et al. in 2017 [57]. In 2020, by modifying the  $[\text{Re}(\text{bpy})(\text{CO})_3\text{Cl}]$  complex with an anchoring group,  $-\text{PO}_3\text{H}_2$  (Figure 6b), Hamm et al. successfully loaded it with a cobalt catalyst,  $[\text{Co}(\text{DMTPy}-\text{O}-\text{benzyl}-3,5\text{-bis}(\text{MePO}_3\text{H}))]$ , on  $\text{ZrO}_2$ , demonstrating the possibility of constructing heterogeneous photocatalytic systems using Re photosensitizers [58].

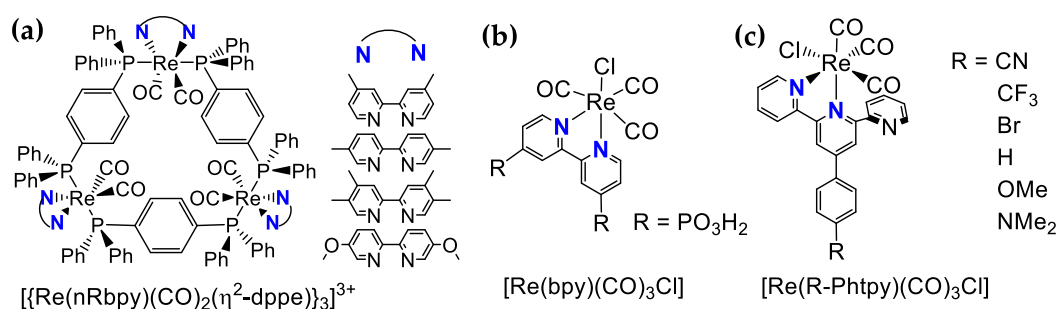


**Figure 6.** Chemical structures of the (a) Rhenium(I) trinuclear -based, (b)  $[\text{Re}(4,4'\text{-PO}_3\text{H}_2\text{-bpy})(\text{CO})_3\text{Cl}]$ -based, and (c) Rhenium(I) tricarbonyl photosensitizers in this review.

Recently, Fernandez-Terán et al. reported the feasibility of tuning the properties of rhenium(I) tricarbonyl complexes through changing the substituent with various groups (i.e., CN,  $\text{CF}_3$ , Br, H, OMe, and  $\text{NMe}_2$ ) as shown in Figure 6c. It was found that the complex with the most electron-donating group,  $\text{NMe}_2$ , showed a notable lifetime of 380 ns and a TON of over 2100 [59]. This is the first example of applying the  $^3\text{ILCT}$  state of a rhenium(I) tricarbonyl complex as a stable photosensitizer.

These studies implied that Re-based complexes are good candidates for replacing ruthenium as photosensitizers for stable photocatalytic reactions.

Table 1 summarized the properties of noble-metal-based photosensitizers in this review, as shown below.

**Table 1.** Summary of the properties of the partial noble-metal-based photosensitizers in this review.

Photosensitizer	Solvent *	$E_{1/2}$ (V)	$\lambda_{\text{abs}}$ (nm)	$\lambda_{\text{em}}$ (nm)	$\tau_{\text{avg}}$	$\Phi$	TON <sup>h</sup>	TOF <sup>h</sup>	Reference
$[\text{Ru}(\text{bpy})_3]^{2+}$	0.10 M $\text{HClO}_4$	1.26 <sup>a</sup>	454	611	580 ns	0.042	/	/	[24]
$[\text{Ru}(4\text{-CF}_3\text{-4'-PO}_3\text{H}_2\text{-bpy})_3]^{2+}$	0.10 M $\text{HClO}_4$	1.60 <sup>a</sup>	461	624	667 ns	0.0334	75	0.24/s	[24]
$[\text{Ru}(4\text{-CF}_3\text{-5'-PO}_3\text{H}_2\text{-bpy})_3]^{2+}$	0.10 M $\text{HClO}_4$	1.60 <sup>a</sup>	468	640	222 ns	0.0123	90	0.19/s	[24]
$[\text{Ru}(4\text{-PO}_3\text{H}_2\text{-bpy})_3]^{2+}$	0.10 M $\text{HClO}_4$	1.34 <sup>a</sup>	458	628	534 ns	0.0379	70	0.21/s	[24]
$[\text{Ru}(5\text{-PO}_3\text{H}_2\text{-bpy})_3]^{2+}$	0.10 M $\text{HClO}_4$	1.34 <sup>a</sup>	467	640	147 ns	0.0128	55	0.21/s	[24]
$[\text{Ru}(4\text{-CF}_3\text{-bpy})_3]^{2+}$	0.10 M $\text{HClO}_4$	1.51 <sup>a</sup>	455	617	731 ns	0.0141	85	0.21/s	[24]
$[\text{Ru}(5\text{-CF}_3\text{-bpy})_3]^{2+}$	0.10 M $\text{HClO}_4$	1.53 <sup>a</sup>	464	630	258 ns	0.0238	140	0.24/s	[24]
$[\text{Ru}(\text{phen})_3]^{2+}$	$\text{CH}_3\text{CN}$	1.29 <sup>b</sup>	447	595	0.4 $\mu\text{s}$	/	66	5.5/10 h	[45]
$[\text{Ru}(\text{phen})_2(5\text{-pyrenylphen})_3]^{2+}$	$\text{CH}_3\text{CN}$	1.36 <sup>b</sup>	447	595	32 $\mu\text{s}$	/	452	37.6/10 h	[45]
$[\text{Ru}(\text{phen})_2(3\text{-pyrenylphen})_3]^{2+}$	$\text{CH}_3\text{CN}$	1.36 <sup>b</sup>	391	632	68.2 $\mu\text{s}$	/	1120	93.3/10 h	[45]
$[\text{Ru}(\text{phen})_2(3\text{-pyrenyl ethynylphen})_3]^{2+}$	$\text{CH}_3\text{CN}$	1.40 <sup>b</sup>	415	668	118.7 $\mu\text{s}$	/	120	10/10 h	[45]
$[\text{Ru}(\text{bpy})_2(\text{dppz})]^{2+}$	$\text{CH}_3\text{CN}$	0.84 <sup>c,e</sup>	450	/	/	/	/	/	[49]
$[\text{Ru}(\text{bpy})_2(\text{oxo-dppqp})]^{2+}$	$\text{CH}_3\text{CN}$	0.86 <sup>c,e</sup>	417	/	/	/	/	/	[49]
$[\text{Ir}(\text{ppy})_2(\text{bpy})]^+$	$\text{CH}_3\text{CN}$	1.25 <sup>d</sup>	/	585	/	/	275	/	[50]
$[\text{Ir}(\text{ppy})_2(\text{phen})]^+$	$\text{CH}_3\text{CN}$	1.24 <sup>d</sup>	/	579	/	/	195	/	[50]
$[\text{Ir}(\text{ppy})_2(\text{dphen})]^+$	$\text{CH}_3\text{CN}$	1.23 <sup>d</sup>	/	587	/	/	/	/	[50]

Table 1. Cont.

Photosensitizer	Solvent *	E <sub>1/2</sub> (V)	λ <sub>abs</sub> (nm)	λ <sub>em</sub> (nm)	τ <sub>avg</sub>	Φ	TON <sup>h</sup>	TOF <sup>h</sup>	Reference
[Ir(ppy) <sub>2</sub> (NacNac <sup>Cy</sup> )] <sup>+</sup>	CH <sub>3</sub> CN	−0.39 <sup>c</sup>	/	/	/	/	/	/	[54]
[Ir(ppy) <sub>2</sub> (NacNac <sup>NMe2</sup> )] <sup>+</sup>	CH <sub>3</sub> CN	−0.26 <sup>c</sup>	511 <sup>f</sup>	634	0.75 μs	0.16	/	/	[53]
[Ir(ppy) <sub>2</sub> (NacNac <sup>Me</sup> )] <sup>+</sup>	CH <sub>3</sub> CN	−0.07 <sup>c</sup>	460 <sup>f</sup>	595	0.2 μs	0.053	/	/	[53]
[Ir(ppy) <sub>2</sub> (NacNac <sup>OEt</sup> )] <sup>+</sup>	CH <sub>3</sub> CN	0.03 <sup>c</sup>	456 <sup>f</sup>	571	2 μs	0.23	/	/	[53]
[Ir(ptz) <sub>2</sub> (NacNac <sup>NMe2</sup> )] <sup>+</sup>	CH <sub>3</sub> CN	−0.22 <sup>c</sup>	380	576	0.13 μs	0.025	/	/	[55]
[Ir(ptz) <sub>2</sub> (NacNac <sup>Cy</sup> )] <sup>+</sup>	CH <sub>3</sub> CN	−0.41 <sup>c</sup>	375	642	0.068 μs	0.0032	/	/	[55]
[Ir(pmb) <sub>2</sub> (NacNac <sup>NMe2</sup> )] <sup>+</sup>	CH <sub>3</sub> CN	−0.26 <sup>c</sup>	430	591	0.85 μs	0.039	/	/	[55]
[Ir(pmb) <sub>2</sub> (NacNac <sup>Cy</sup> )] <sup>+</sup>	CH <sub>3</sub> CN	−0.43 <sup>c</sup>	439	675	0.12 μs	0.0027	/	/	[55]
[[Re(4-dmbpy)(CO) <sub>2</sub> (η <sup>2</sup> -dppe)] <sub>3</sub> ] <sup>3+</sup>	DMF	−1.73 <sup>g</sup>	398	598	1.57 μs	0.12	19.68	/	[56]
[[Re(5-dmbpy)(CO) <sub>2</sub> (η <sup>2</sup> -dppe)] <sub>3</sub> ] <sup>3+</sup>	DMF	−1.82 <sup>g</sup>	390	561	2.32 μs	0.36	14.2	/	[56]
[[Re(4,5-dmbpy)(CO) <sub>2</sub> (η <sup>2</sup> -dppe)] <sub>3</sub> ] <sup>3+</sup>	DMF	−1.91 <sup>g</sup>	384	545	3.58 μs	0.60	6.31	/	[56]
[[Re(4-OMebpy)(CO) <sub>2</sub> (η <sup>2</sup> -dppe)] <sub>3</sub> ] <sup>3+</sup>	DMF	−1.89 <sup>g</sup>	380	543	7.77 μs	0.66	2.13	/	[56]
Re(CN-Phtpy)(CO) <sub>3</sub> Cl	DMF	−1.61 <sup>c</sup>	389	667	0.582 ns	/	/	/	[59]
Re(CF <sub>3</sub> -Phtpy)(CO) <sub>3</sub> Cl	DMF	−1.66 <sup>c</sup>	387	666	0.79 ns	/	/	/	[59]
Re(Br-Phtpy)(CO) <sub>3</sub> Cl	DMF	−1.70 <sup>c</sup>	382	663	1.35 ns	/	/	/	[59]
Re(H-Phtpy)(CO) <sub>3</sub> Cl	DMF	−1.73 <sup>c</sup>	380	652	1.53 ns	/	580	~2.5/s	[59]
Re(OMe-Phtpy)(CO) <sub>3</sub> Cl	DMF	−1.77 <sup>c</sup>	378	647	2.26 ns	/	/	/	[59]
Re(NMe <sub>2</sub> -Phtpy)(CO) <sub>3</sub> Cl	DMF	−1.81 <sup>c</sup>	425	532	380 ns	/	2130	~150/s	[59]

\* Measurements were performed on the listed solvent unless otherwise noted. <sup>a</sup> Potential versus NHE in 0.1 M HClO<sub>4</sub>. <sup>b</sup> Ferrocene (Fc) was used as an internal reference (E<sub>1/2</sub> = + 0.40 V (Fc<sup>+</sup>/Fc) vs. SCE). <sup>c</sup> Potential vs. Fc<sup>+/0</sup>. <sup>d</sup> Potential vs. SCE. <sup>e</sup> In DMF. <sup>f</sup> In THF. <sup>g</sup> Potential vs. Ag/AgNO<sub>3</sub>. <sup>h</sup> 20 μM PSs.

#### 4. Noble-Metal-Free Photosensitizers

Over the last decade, the investigation of photosensitizers based on nonprecious transition metals dramatically increased owing to their favorable (photo)physical properties, high earth abundancy, and low cost. Table 2 shows the earth abundancy of the metal elements mentioned in this review. However, due to the fact of these photosensitizers' feature of unwanted nonradiative decay, they generally perform worse than noble-metal-based photosensitizers in terms of photophysical properties (i.e., MLCT and lifetime) and redox potential [60]. Nevertheless, nonprecious transition metal complexes have shown highly attractive potentials in photocatalytic hydrogen production and CO<sub>2</sub> reduction [61]. In the subsequent sections, recent advances in noble-metal-free photosensitizers from low atomic number to high atomic number are summarized.

**Table 2.** Earth abundance (in mass percent) of the metal elements mentioned in this review [62]. Adapted with permission from J. Am. Chem. Soc. 2018, 140, 42, 13522–13533. Copyright 2018 American Chemical Society.

Element	Abundance	Element	Abundance
Ru	10 <sup>−6</sup>	Mn	0.091
Re	10 <sup>−7</sup>	Fe	4.7
Os	5 × 10 <sup>−7</sup>	Ni	7.2 × 10 <sup>−3</sup>
Ir	10 <sup>−7</sup>	Cu	0.005
Pt	10 <sup>−6</sup>	Zn	0.007

##### 4.1. Mn-Based Photosensitizers

Manganese plays an essential role in absorbing light in natural photosynthesis process; hence, it has inspired the development of Mn-based nanomaterials for photocatalysis [63–66]. However, due to the fact of their intrinsic nonradiative decay of excited states, it is still a grand challenge to make Mn-based complexes luminescent and photoactive.

Wenger et al. recently reported a family of novel isocyanide Mn(I) complexes, [Mn(L<sup>bi</sup>)<sub>3</sub>]<sup>+</sup> and [Mn(L<sup>tri</sup>)<sub>2</sub>]<sup>+</sup>, that exhibited the first example of manganese complexes with luminescent MLCT and photo-reactivity at room temperature [67,68] as shown in Figure 7. This series of

Mn-based homoleptic photosensitizers is air-stable and nontoxic, and the redox potential of Mn(I/II) is reversible. Spectrum studies gave a <sup>1</sup>MLCT absorption wavelength at ~390 nm and an emission wavelength at ~500 nm. These complexes have been successfully applied in energy conversion reactions. Unlike traditional energy transfer pathways (i.e., MLCT, LMCT, and MC excited states), their study provide the attractive possibility of realizing the triplet-energy-transfer photo-reactivity by a ligand-centered  $\pi-\pi^*$  state.

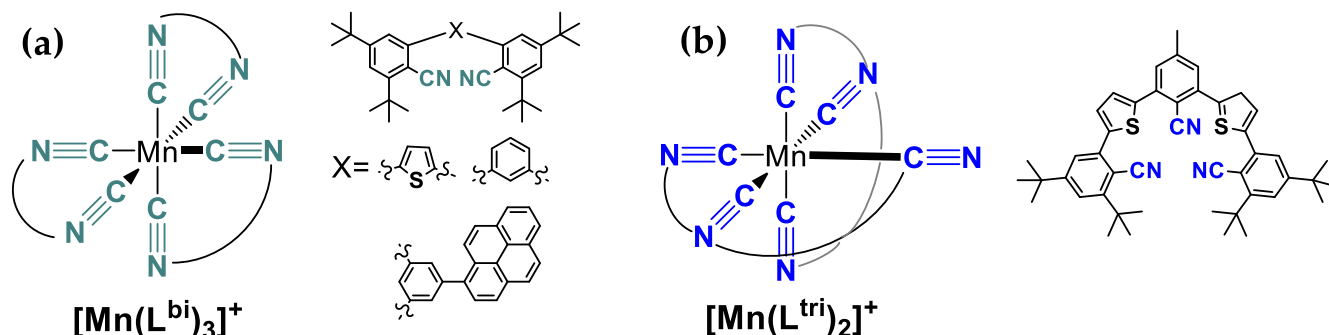


**Figure 7.** Chemical structures of the (a)  $[\text{Mn}(\text{L}^{\text{bi}})_3]^+$ -based and (b)  $[\text{Mn}(\text{L}^{\text{tri}})_2]^+$ -based photosensitizers and corresponding ligands in this review.

Currently developed Mn-based complexes are not comparable with traditional noble-metal-based photosensitizers in terms of excited-state lifetime or driving force for photocatalytic reactions, but these studies open new avenues to exploring cheap bio-inspired molecules for artificial photosynthesis.

#### 4.2. Fe-Based Photosensitizers

Iron is the most earth-abundant transition metal element [62]. Therefore, in recent years, much attention has been paid toward developing Fe-based photosensitizers considering their low cost. Inspired by Ru(II) polypyridyl complexes, which show decent photophysical properties [38], iron(II) polypyridyl photosensitizers have been widely studied [69–74].

Kunnus et al. recently reported a series of  $[\text{Fe}(\text{N}^{\wedge}\text{N})(\text{CN})_4]^{2-}$ -type photosensitizers, where  $\text{N}^{\wedge}\text{N}$  represents 2,2'-bipyridine (bpy); 2,3-bis(2-pyridyl)pyrazine (bpyz); 2,2'-bipyrimidine (bpym), respectively (Figure 8a), and studied the solvent effect on the chemical properties as well as the MLCT excitation energy dependence of the <sup>3</sup>MLCT lifetime. Femtosecond transient absorption (TA) data and td-DFT calculations revealed the tunability of the excited-state relaxation mechanisms and charge transfer lifetimes, which increased from 0.22 to 16.9 ps with an increasing number of nitrogen in the ligand.

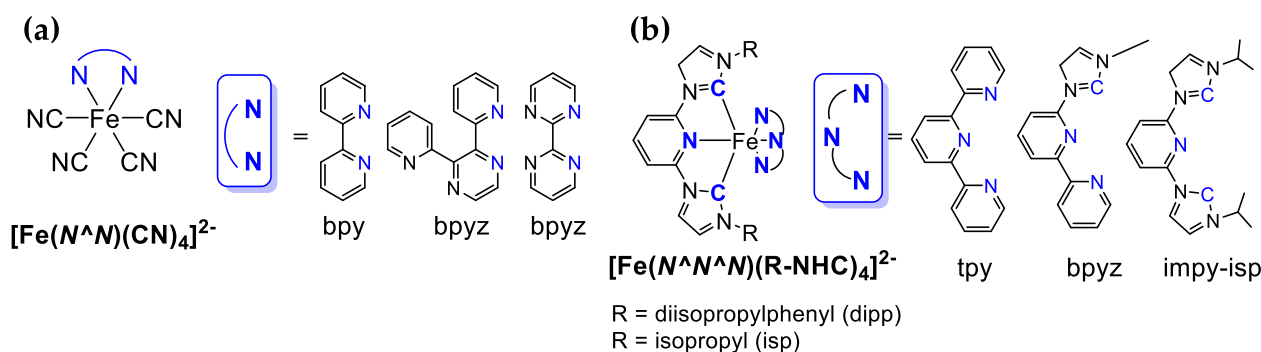


**Figure 8.** Chemical structures of the (a)  $[\text{Fe}(\text{N}^{\wedge}\text{N})(\text{CN})_4]^{2-}$ -based and (b)  $[\text{Fe}(\text{N}^{\wedge}\text{N}^{\wedge}\text{N})(\text{R}-\text{NHC})_4]^{2-}$ -based photosensitizers and corresponding ligands in this review.

In addition to iron(II) polypyridyl complexes, iron (II) N-heterocyclic carbene (NHC) complexes (Figure 8b) have been extensively investigated as photosensitizers [75–79]. The strong bonding between iron and the carbene ligands leads to increased ligand-field splitting, resulting in the destabilization of the MC states. As a consequence, Fe(II)-NHC-type photosensitizers present prominent properties such as long excited-state lifetimes and high charge transfer abilities [77]. Bauer et al. studied the relationships between the number of NHC ligands and the photophysical properties of Fe photosensitizers. An increasing trend in the  $^3\text{MLCT}$  lifetime was found when there was an increase in the number of NHC ligands [78]. In their follow-up study, the excited-state dynamics of  $[\text{Fe}^{\text{II}}(\text{tpy})(\text{pyz-NHC})]^{2+}$  was investigated. The results of intersystem crossing and triplet dynamics further interpreted the excellent performance of Fe(II)-NHC photosensitizers.

At present, the photophysical properties and stability of Fe-based photosensitizers are not comparable to Ru-based complexes. However, its high earth-abundance and low cost attract continuous attention. Future work on Fe-based photosensitizers will focus on extending their charge-separated state and improving their photostability.

#### 4.3. Cu-Based Photosensitizers

Copper-based photosensitizers have been popular since the 1970s because of their MLCT nature and high earth abundance [80–84]. With the extensive study of copper complexes, Cu-based photosensitizers possessing considerable properties and good performances have increasingly been developed. Unlike other abundant transition metals, copper complexes have a filled  $d$  subshell, which blocks the formation of a metal-centered excited state. Therefore, many copper (I) complexes show MLCT luminescence [60]. As a result of its sustainability and photophysical properties, in recent years, copper is replacing ruthenium for use as molecular photosensitizers in dye-sensitized solar cells (DSSCs) [85]. Housecroft and Constable have reviewed the progress of copper(I)-containing DSSCs [86].

Mulfort et al. developed and studied a series of copper(I) diimine photosensitizers based on the HETPHEN method [87,88] and immobilized these photosensitizers on the metal oxide surface via carboxylate groups [26]. The CuHETPHEN strategy provides many more possibilities for tuning the structures and properties of copper photosensitizers. These discoveries related to copper complexes promote important improvements in Cu-based photosensitizers and further increase their potential applications in the solar energy conversion industry. The photochemical processes of copper-based photosensitizers have been well explored by advanced technologies such as spectroscopies [89–92]. In general, ground-state copper complex is excited into a singlet MLCT state, which then undergoes a flattening distortion and becomes triplet MLCT state. Depending on the coordination ability of the solvent, the  $^3\text{MLCT}$  state complex may or may not bind the solvent molecule. After experiencing a strong interaction, the complex recovers to the ground state as shown in Figure 9. Chen et al. reviewed the photocatalytic mechanisms of copper(I) diimine complexes and their developments and applications in solar energy conversion in 2015 [93].

From a chelating element perspective, there are four types of copper (I) photosensitizers:  $\text{Cu}(\text{N}^{\wedge}\text{N})(\text{N}^{\wedge}\text{N})$ ,  $\text{Cu}(\text{N}^{\wedge}\text{N})(\text{P}^{\wedge}\text{P})$ ,  $\text{Cu}(\text{N}^{\wedge}\text{N})(\text{N}^{\wedge}\text{P})$ , and  $\text{Cu}(\text{N}^{\wedge}\text{P})(\text{N}^{\wedge}\text{P})$  as shown in Figure 10a. In terms of  $\text{Cu}(\text{N}^{\wedge}\text{N})(\text{N}^{\wedge}\text{N})$ -type photosensitizers, Hadt et al. quantified the entatic effects of several  $[\text{Cu}(\text{phen-X})_2]^+$  complexes, where X are the 2,9-alkyl substitutions, and correlations were found between the lifetime, the excited-state relaxation energy, the reorganization energy, and the energy gap [94]. Castellano et al. successfully prepared various Cu-phen MLCT photosensitizers featuring bulky substituents. Impressive photophysical properties ( $\tau = 1.5 \mu\text{s}$ ,  $\Phi = 2.6\%$  in acetonitrile) were discovered when used dchtmp as the ligand. Their C–C radical coupling photochemistry strategy broke through the traditional limit of steric bulk possibility for homoleptic Cu(I) complexes [95,96].

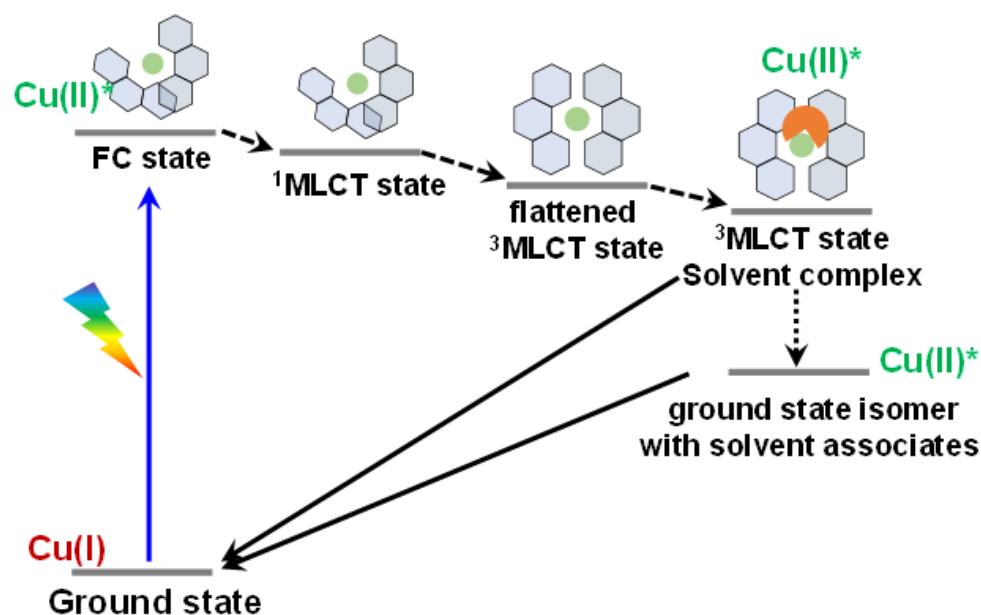


Figure 9. Photochemical process of copper-based photosensitizers (Cu(I): ground state, Cu(II)\*: excited state).

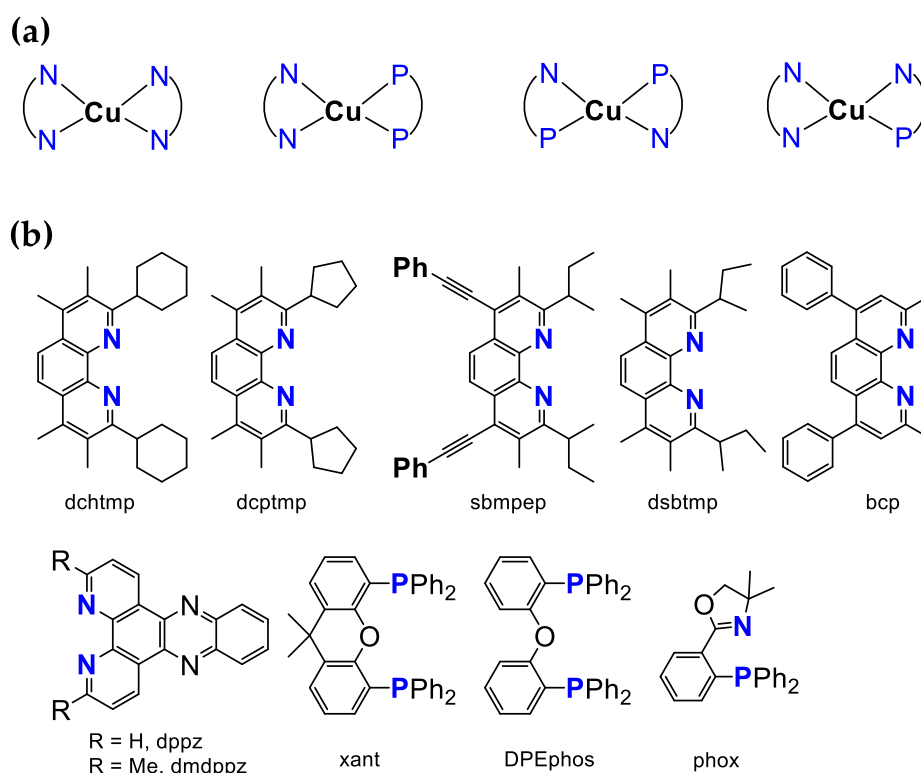


Figure 10. Chemical structures of the (a) Cu-based photosensitizers and (b) corresponding ligands in this review.

In recent years, scientists have aimed at replacing nitrogen with phosphines in transition-metal-based photosensitizers. Generally, the introduction of phosphines usually brings about a higher stability and lower redox potentials [97–102]. Karnahl et al. prepared a hetero-bidentate P<sup>+</sup>N ligand, phox, and improved the performance of Cu-based photosensitizers [100]. Ishitani et al. synthesized [Cu(dmp)(DPEphos)]<sup>+</sup> complexes, where DPEphos is 2-(diphenylphosphino)phenyl]ether, for photocatalytic CO<sub>2</sub> reduction. By com-

paring the properties of a series of  $[\text{Cu}(\text{N}^{\wedge}\text{N})(\text{DPEphos})]^+$  photosensitizers, the influences of expending  $\pi$ -systems were discovered [103]. Dietzek et al. [91] and Karnahl et al. [104] recently studied the extended  $\pi$ -system effect on the properties of  $[\text{Cu}(\text{xant})(\text{dppz})]^+$  and  $[\text{Cu}(\text{xant})(\text{dmdppz})]^+$ . The extended  $\pi$ -system provided unusual properties such as broadening and a red-shift of the MLCT absorption and a prolonged lifetime. Dietzek et al., in particular, studied the effect of the electronic structures of Cu(I) photosensitizers containing phosphines [105]. Their study on the Franck–Condon region of heteroleptic Cu(I) complexes provides new theoretical principles for designing Cu-based photosensitizers. Bruggeller et al. recently reviewed the development of photosensitizers with phosphines and summarized the influence of phosphines on the properties of photosensitizers [106].

Among the aforementioned noble-metal-free complexes, the copper family has the greatest potential to replace noble-metal photosensitizers as indicated by their promising photophysical properties such as long lifetimes. Nevertheless, their poor chemical stability and environmental sensitivity (to pH value, humidity, etc.) impede their broad applications in energy conversion. Efforts towards improving these properties will be the focus of future research.

#### 4.4. Other Photosensitizers

Other types of metal-based photosensitizers are less common than manganese, iron, and copper. Inspired by natural photosynthesis, many of these photosensitizers (Figure 11) are based on porphyrin and its derivatives, which itself is a biomimetic light-harvesting molecule [107–109]. Poddutoori et al. reviewed unique aluminum (III) porphyrin complexes, which can act as either electron donor or electron acceptor in donor–acceptor systems because of their redox and optical properties [110]. Park et al. creatively designed positively charged Zn and neutral Sn porphyrins complexes,  $[\text{ZnTMePyP}_4^+]\text{Cl}_4$  and  $\text{Sn}(\text{OH})_2\text{TPyP}$ ,  $\text{Sn}(\text{Cl}_2)\text{TPP}-[\text{COOMe}]_4$ , and  $\text{Sn}(\text{Cl}_2)\text{TPP}-[\text{PO}(\text{OEt})_2]_4$ , as photosensitizers for  $\text{H}_2$  evolution. Their study clearly demonstrated the influence of pH value as well as solution concentration. It also showed that the photocatalytic process can be realized by oxidative quenching of the photosensitizer [111]. The results of this study shed light on designing and synthesizing metal-containing photosensitizers based on porphyrin. Willner et al. developed an all-DNA system with Zn (II)-protoporphyrin IX ( $\text{Zn}^{\text{II}}\text{PPIX}$ ) as a photosensitizer [112]. In this mimic PSI system,  $\text{Zn}^{\text{II}}\text{PPIX}$  presented effective photoinduced electron transfer (ET). Their report provides a versatile approach for designing supramolecular photosensitizers.

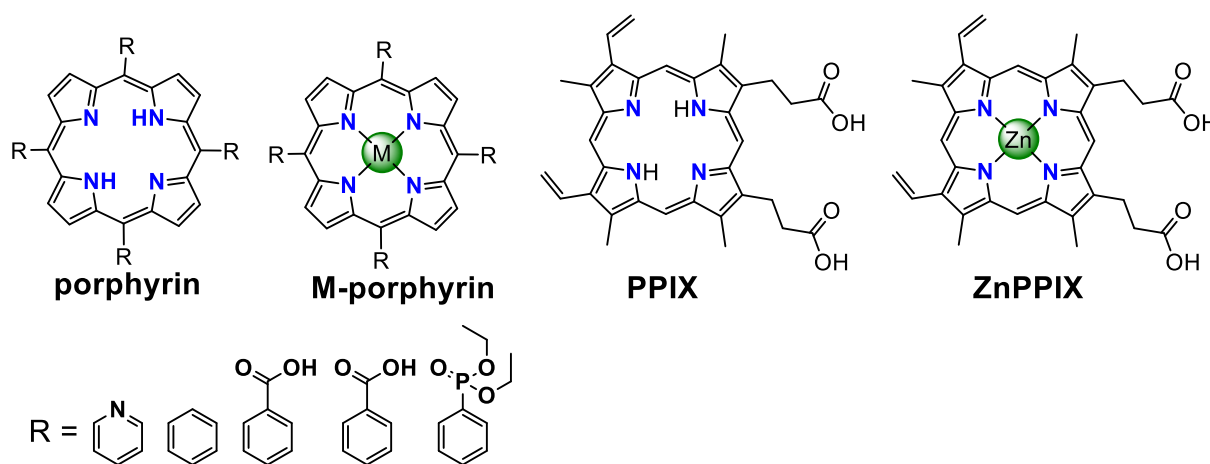


**Figure 11.** Chemical structures of porphyrin, M-porphyrin (M = Al, Zn, and Sn), protoporphyrin IX (PPIX), and ZnPPIX.

Detailed parameters for some of above noble-metal-free photosensitizers are summarized in Table 3.

**Table 3.** Summary of the properties of the partial noble-metal-free photosensitizers in this review.

Photosensitizer	Solvent	$E_{1/2}$ (V)	$\lambda_{abs}$ (nm)	$\lambda_{em}$ (nm)	$\tau_{avg}$	$\Phi$	Reference
[Mn(L <sup>bi</sup> ) <sub>3</sub> ] <sup>+</sup>	CH <sub>3</sub> CN	1.05 <sup>a</sup>	385	485	0.74 ns	0.05%	[68]
[Mn(L <sup>tri</sup> ) <sub>2</sub> ] <sup>+</sup>	CH <sub>3</sub> CN	1.00 <sup>a</sup>	395	525	1.73 ns	0.03%	[68]
[Fe(bpy)(CN) <sub>4</sub> ] <sup>2-</sup>	CH <sub>3</sub> OH	/	514 <sup>b</sup>	/	0.22 ps	/	[113]
[Fe(bpyz)(CN) <sub>4</sub> ] <sup>2-</sup>	CH <sub>3</sub> OH	/	590 <sup>b</sup>	/	0.61 ps	/	[113]
[Fe(bpym)(CN) <sub>4</sub> ] <sup>2-</sup>	CH <sub>3</sub> OH	/	608 <sup>b</sup>	/	16.9 ps	/	[113]
[Fe(tpy)(dipp-NHC)] <sup>2-</sup>	CH <sub>3</sub> CN	0.56 <sup>c</sup>	379, 503, 538	/	/	/	[78]
[Fe(isp-NHC) <sub>2</sub> ] <sup>2-</sup>	CH <sub>3</sub> CN	0.43 <sup>c</sup>	392, 458	/	/	/	[78]
[Fe(bpyz)(dipp-NHC)] <sup>2-</sup>	CH <sub>3</sub> CN	0.46 <sup>c</sup>	376, 409, 466, 506, 538	/	/	/	[78]
[Cu(dsbtmp) <sub>2</sub> ] <sup>+</sup>	CH <sub>3</sub> CN	0.428 <sup>c</sup>	445	649	1.5 $\mu$ s	2.9%	[95]
[Cu(dchtmp) <sub>2</sub> ] <sup>+</sup>	CH <sub>3</sub> CN	0.43 <sup>c</sup>	/	650	1.5 $\mu$ s	2.6%	[95]
[Cu(sbmpep) <sub>2</sub> ] <sup>+</sup>	CH <sub>2</sub> Cl <sub>2</sub>	0.69 <sup>c</sup>	491	687	1.4 $\mu$ s	2.7%	[96]
[Cu(xant)(dppz)] <sup>+</sup>	CH <sub>3</sub> CN	0.815, 1.026 <sup>c</sup>	376, 394	/	4380 ns	/	[104]
[Cu(xant)(dmdppz)] <sup>+</sup>	CH <sub>3</sub> CN	0.926, 1.228 <sup>c</sup>	383, 400	/	1250 ns, 3785 ns	/	[104]
[Cu(xant)(dmphen)] <sup>+</sup>	CH <sub>3</sub> CN	0.82 <sup>c</sup>	378	/	64 ns	/	[104]
[Cu(DPEphos)(bcp)] <sup>+</sup>	CH <sub>3</sub> CN	/	384	590	0.99 $\mu$ s	2.7%	[103]
[ZnTMePyP <sub>4</sub> ] <sup>+</sup> Cl <sub>4</sub>	1:1 CH <sub>3</sub> CN/H <sub>2</sub> O	1.28 <sup>d</sup>	438	627/667	85 $\mu$ s	/	[111]
Sn(OH) <sub>2</sub> TPyP	1:1 CH <sub>3</sub> CN/H <sub>2</sub> O	1.38 <sup>d</sup>	417	597/650	78 $\mu$ s	/	[111]
Sn(Cl <sub>2</sub> )TPP-[COOMe] <sub>4</sub>	1:1 CH <sub>3</sub> CN/H <sub>2</sub> O	1.29 <sup>d</sup>	425	604/660	70 $\mu$ s	/	[111]
Sn(Cl <sub>2</sub> )TPP-[PO(OEt) <sub>2</sub> ] <sub>4</sub>	1:1 CH <sub>3</sub> CN/H <sub>2</sub> O	1.32 <sup>d</sup>	424	605/659	/	/	[111]

<sup>a</sup> Data obtained in dichloromethane at 20 °C, potential versus SCE in CH<sub>3</sub>CN. <sup>b</sup> Data were calculated from  $\frac{1240}{E_{\nu}(eV)}$ .

<sup>c</sup> Potential versus Fc<sup>+0</sup> standard in CH<sub>3</sub>CN. <sup>d</sup> Potential versus Fc<sup>+0</sup> standard in DMF.

## 5. Conclusions and Outlook

This review endeavored to summarize the evaluating parameters and recent work on metal-based molecular photosensitizers. Noble-metal-based photosensitizers, such as ruthenium, iridium, and rhenium, are the most investigated metal-based photosensitizers and many reviews on these photosensitizers are available; hence, here, recent advances in noble-metal-based photosensitizers were briefly reviewed. These photosensitizers, however, are scarce, expensive, and toxic to humans. Thus, noble-metal-free photosensitizers have become research hotspots in the solar energy conversion field. Due to the fact of their valuable photophysical properties and their charge-separation ability to induce photochemistry, manganese, iron, and copper, they have recently received particular attention. Some photosensitizers were found to be active, but further work in promoting their higher efficiency and stronger stability as well as a greater understanding of their mechanisms are needed for their large-scale industrial application. In addition to the metal-based photosensitizers that were highlighted in this review, biomolecular photosensitizers, such as from natural bacterial sources, are another attractive alternative to expensive metal-based photosensitizers.

**Funding:** This research received no external funding.

**Data Availability Statement:** Not applicable.

**Acknowledgments:** Contribution from Lijuan Wang who collected publication data in Figure 1. Support from Shanghai Outstanding Academic Leaders Program.

**Conflicts of Interest:** We declare that we have no financial and personal relationships with other people or organizations that can inappropriately influence our work, there is no professional or other personal interest of any nature or kind of in any product, service and/or company that could be construed as influencing the review entitled.

## References

1. Kharecha, P.A.; Hansen, J.E. Implications of “peak oil” for atmospheric CO<sub>2</sub> and climate. *Glob. Biogeochem. Cycles* **2008**, *22*, GB3012. [CrossRef]
2. Stern, D.I.; Kander, A. The role of energy in the industrial revolution and modern economic growth. *Energy J.* **2012**, *33*, 3. [CrossRef]
3. Mayumi, K. Temporary emancipation from land: From the industrial revolution to the present time. *Ecol. Econ.* **1991**, *4*, 35–56. [CrossRef]

4. Dincer, I. Renewable energy and sustainable development: A crucial review. *Renew. Sust. Energ. Rev.* **2000**, *4*, 157–175. [[CrossRef](#)]
5. Vakulchuk, R.; Overland, I.; Scholten, D. Renewable energy and geopolitics: A review. *Renew. Sust. Energ. Rev.* **2020**, *122*, 109547. [[CrossRef](#)]
6. Gielen, D.; Boshell, F.; Saygin, D.; Bazilian, M.D.; Wagner, N.; Gorini, R. The role of renewable energy in the global energy transformation. *Energy Strategy Rev.* **2019**, *24*, 38–50. [[CrossRef](#)]
7. Ren, D.; Loo, N.W.X.; Gong, L.; Yeo, B.S. Continuous production of ethylene from carbon dioxide and water using intermittent sunlight. *ACS Sustain. Chem. Eng.* **2017**, *5*, 9191–9199. [[CrossRef](#)]
8. Kim, D.; Sakimoto, K.K.; Hong, D.; Yang, P. Artificial photosynthesis for sustainable fuel and chemical production. *Angew. Chem. Int. Ed.* **2015**, *54*, 3259–3266. [[CrossRef](#)]
9. Ji, X.; Su, Z.; Wang, P.; Ma, G.; Zhang, S. Integration of artificial photosynthesis system for enhanced electronic energy-transfer efficacy: A case study for solar-energy driven bioconversion of carbon dioxide to methanol. *Small* **2016**, *12*, 4753–4762. [[CrossRef](#)]
10. Jia, Y.; Xu, Y.; Nie, R.; Chen, F.; Zhu, Z.; Wang, J.; Jing, H. Artificial photosynthesis of methanol from carbon dioxide and water via a Nile red-embedded TiO<sub>2</sub> photocathode. *J. Mater. Chem. A* **2017**, *5*, 5495–5501. [[CrossRef](#)]
11. Stoll, T.; Castillo, C.E.; Kayanuma, M.; Sandroni, M.; Daniel, C.; Odobel, F.; Fortage, J.; Collomb, M.N. Photo-induced redox catalysis for proton reduction to hydrogen with homogeneous molecular systems using rhodium-based catalysts. *Coord. Chem. Rev.* **2015**, *304*, 20–37. [[CrossRef](#)]
12. Puntoriero, F.; La Ganga, G.; Cancelliere, A.M.; Campagna, S. Recent progresses in molecular-based artificial photosynthesis. *Curr. Opin. Green Sustain. Chem.* **2022**, *36*, 100636. [[CrossRef](#)]
13. Berardi, S.; Drouet, S.; Francàs, L.; Gimbert-Suriñach, C.; Guttentag, M.; Richmond, C.; Stoll, T.; Llobet, A. Molecular artificial photosynthesis. *Chem. Soc. Rev.* **2014**, *43*, 7501–7519. [[CrossRef](#)]
14. Wang, C.; O'Hagan, M.P.; Willner, B.; Willner, I. Bioinspired artificial photosynthetic systems. *Chem. Eur. J.* **2022**, *28*, e202103595. [[CrossRef](#)]
15. Barber, J.; Tran, P.D. From natural to artificial photosynthesis. *J. R. Soc. Interface* **2013**, *10*, 20120984. [[CrossRef](#)]
16. Khalil, M.; Gunlazuardi, J.; Ivandini, T.A.; Umar, A. Photocatalytic conversion of CO<sub>2</sub> using earth-abundant catalysts: A review on mechanism and catalytic performance. *Renew. Sust. Energ. Rev.* **2019**, *113*, 109246. [[CrossRef](#)]
17. Puntoriero, F.; Sartorel, A.; Orlandi, M.; La Ganga, G.; Serroni, S.; Bonchio, M.; Scandola, F.; Campagna, S. Photoinduced water oxidation using dendrimeric Ru (II) complexes as photosensitizers. *Coord. Chem. Rev.* **2011**, *255*, 2594–2601. [[CrossRef](#)]
18. Dogutan, D.K.; Nocera, D.G. Artificial photosynthesis at efficiencies greatly exceeding that of natural photosynthesis. *Acc. Chem. Res.* **2019**, *52*, 3143–3148. [[CrossRef](#)]
19. Wang, H.; Zhang, L.; Chen, Z.; Hu, J.; Li, S.; Wang, Z.; Liu, J.; Wang, X. Semiconductor heterojunction photocatalysts: Design, construction, and photocatalytic performances. *Chem. Soc. Rev.* **2014**, *43*, 5234–5244. [[CrossRef](#)]
20. Yuan, Y.J.; Yu, Z.T.; Chen, D.Q.; Zou, Z.G. Metal-complex chromophores for solar hydrogen generation. *Chem. Soc. Rev.* **2017**, *46*, 603–631. [[CrossRef](#)]
21. Shon, J.H.; Teets, T.S. Molecular photosensitizers in energy research and catalysis: Design principles and recent developments. *ACS Energy Lett.* **2019**, *4*, 558–566. [[CrossRef](#)]
22. Lakowicz, J. *Principles of Fluorescence Spectroscopy*; Springer: New York, NY, USA, 2013.
23. Islam, A.; Sugihara, H.; Arakawa, H. Molecular design of ruthenium (II) polypyridyl photosensitizers for efficient nanocrystalline TiO<sub>2</sub> solar cells. *J. Photochem. Photobiol. A* **2003**, *158*, 131–138. [[CrossRef](#)]
24. Wang, L.; Shaffer, D.W.; Manbeck, G.F.; Polyansky, D.E.; Concepcion, J.J. High-redox-potential chromophores for visible-light-driven water oxidation at low pH. *ACS Catal.* **2019**, *10*, 580–585. [[CrossRef](#)]
25. Vlcek, A.; Dodsworth, E.S.; Pietro, W.J.; Lever, A. Excited state redox potentials of ruthenium diimine complexes; correlations with ground state redox potentials and ligand parameters. *Inorg. Chem.* **1995**, *34*, 1906–1913. [[CrossRef](#)]
26. Eberhart, M.S.; Phelan, B.T.; Niklas, J.; Sprague-Klein, E.A.; Kaphan, D.M.; Gosztola, D.J.; Chen, L.X.; Tiede, D.M.; Poluektov, O.G.; Mulfort, K.L. Surface immobilized copper (i) diimine photosensitizers as molecular probes for elucidating the effects of confinement at interfaces for solar energy conversion. *ChemComm* **2020**, *56*, 12130–12133. [[CrossRef](#)]
27. Marcus, R.A. Electron transfer reactions in chemistry. Theory and experiment. *Rev. Mod. Phys.* **1993**, *65*, 599. [[CrossRef](#)]
28. Lee, H.; Wu, X.; Sun, L. Copper-based homogeneous and heterogeneous catalysts for electrochemical water oxidation. *Nanoscale* **2020**, *12*, 4187–4218. [[CrossRef](#)]
29. Tran, T.T.; Pino, T.; Ha-Thi, M.H. Watching intermolecular light-induced charge accumulation on naphthalene diimide by tris (bipyridyl) ruthenium (II) photosensitizer. *J. Phys. Chem. C* **2019**, *123*, 28651–28658. [[CrossRef](#)]
30. Andreiadis, E.S.; Chavarot-Kerlidou, M.; Fontecave, M.; Artero, V. Artificial photosynthesis: From molecular catalysts for light-driven water splitting to photoelectrochemical cells. *Photochem. Photobiol.* **2011**, *87*, 946–964. [[CrossRef](#)]
31. Chen, H.C.; Hettler, D.G.; Williams, R.M.; van der Vlugt, J.I.; Reek, J.N.; Brouwer, A.M. Platinum (ii)-porphyrin as a sensitizer for visible-light driven water oxidation in neutral phosphate buffer. *Energy Environ.* **2015**, *8*, 975–982. [[CrossRef](#)]
32. Yu, S.; Zeng, Y.; Chen, J.; Yu, T.; Zhang, X.; Yang, G.; Li, Y. Intramolecular triplet-triplet energy transfer enhanced triplet-triplet annihilation upconversion with a short-lived triplet state platinum (II) terpyridyl acetylide photosensitizer. *RSC Adv.* **2015**, *5*, 70640–70648. [[CrossRef](#)]
33. Liu, Y.T.; Li, Y.R.; Wang, X.; Bai, F.Q. Theoretical investigation of N<sup>+</sup>C<sup>-</sup>N-coordinated Pt (II) and Pd (II) complexes for long-lived two-photon photodynamic therapy. *Dyes Pigm.* **2017**, *142*, 55–61. [[CrossRef](#)]

34. Li, C.; Wang, Y.; Li, C.; Xu, S.; Hou, X.; Wu, P. Simultaneously broadened visible light absorption and boosted intersystem crossing in platinum-doped graphite carbon nitride for enhanced photosensitization. *ACS Appl. Mater.* **2019**, *11*, 20770–20777. [[CrossRef](#)]
35. Irikura, M.; Tamaki, Y.; Ishitani, O. Development of a panchromatic photosensitizer and its application to photocatalytic CO<sub>2</sub> reduction. *Chem. Sci.* **2021**, *12*, 13888–13896. [[CrossRef](#)]
36. Lainé, P.P.; Campagna, S.; Loiseau, F. Conformationally gated photoinduced processes within photosensitizer–acceptor dyads based on ruthenium (II) and osmium (II) polypyridyl complexes with an appended pyridinium group. *Coord. Chem. Rev.* **2008**, *252*, 2552–2571. [[CrossRef](#)]
37. Summers, P.A.; Calladine, J.A.; Ghiotto, F.; Dawson, J.; Sun, X.Z.; Hamilton, M.L.; Towrie, M.; Davies, E.S.; McMaster, J.; George, M.W. Synthesis and photophysical study of a [NiFe] hydrogenase biomimetic compound covalently linked to a Re-diimine photosensitizer. *Inorg. Chem.* **2016**, *55*, 527–536. [[CrossRef](#)]
38. Juris, A.; Barigelletti, F.; Balzani, V.; Belser, P.; Von Zelewsky, A. New photosensitizers of the ruthenium-polypyridine family for the water splitting reaction. *Isr. J. Chem.* **1982**, *22*, 87–90. [[CrossRef](#)]
39. Li, H.; Li, F.; Zhang, B.; Zhou, X.; Yu, F.; Sun, L. Visible light-driven water oxidation promoted by host–guest interaction between photosensitizer and catalyst with a high quantum efficiency. *J. Am. Chem. Soc.* **2015**, *137*, 4332–4335. [[CrossRef](#)]
40. Li, H.; Li, F.; Wang, Y.; Bai, L.; Yu, F.; Sun, L. Visible-light-driven water oxidation on a photoanode by supramolecular assembly of photosensitizer and catalyst. *ChemPlusChem* **2016**, *81*, 1056–1059. [[CrossRef](#)]
41. Limburg, B.; Bouwman, E.; Bonnet, S. Rate and stability of photocatalytic water oxidation using [Ru(bpy)<sub>3</sub>]<sup>2+</sup> as photosensitizer. *ACS Catal.* **2016**, *6*, 5273–5284. [[CrossRef](#)]
42. Sheridan, M.V.; Sherman, B.D.; Coppo, R.L.; Wang, D.; Marquard, S.L.; Wee, K.R.; Murakami Iha, N.Y.; Meyer, T.J. Evaluation of chromophore and assembly design in light-driven water splitting with a molecular water oxidation catalyst. *ACS Energy Lett.* **2016**, *1*, 231–236. [[CrossRef](#)]
43. Pickens, R.N.; Neyhouse, B.J.; Reed, D.T.; Ashton, S.T.; White, J.K. Visible light-activated co release and <sup>1</sup>O<sub>2</sub> photosensitizer formation with Ru (II), Mn (I) complexes. *Inorg. Chem.* **2018**, *57*, 11616–11625. [[CrossRef](#)]
44. Ashford, D.L.; Glasson, C.R.; Norris, M.R.; Concepcion, J.J.; Keinan, S.; Brennaman, M.K.; Templeton, J.L.; Meyer, T.J. Controlling ground and excited state properties through ligand changes in ruthenium polypyridyl complexes. *Inorg. Chem.* **2014**, *53*, 5637–5646. [[CrossRef](#)]
45. Wang, P.; Dong, R.; Guo, S.; Zhao, J.; Zhang, Z.M.; Lu, T.B. Improving photosensitization for photochemical CO<sub>2</sub>-to-CO conversion. *Natl. Sci. Rev.* **2020**, *7*, 1459–1467. [[CrossRef](#)]
46. Skaisgirski, M.; Guo, X.; Wenger, O.S. Electron accumulation on naphthalene diimide photosensitized by [Ru (2,2′-Bipyridine)<sub>3</sub>]<sup>2+</sup>. *Inorg. Chem.* **2017**, *56*, 2432–2439. [[CrossRef](#)]
47. Kuss-Petermann, M.; Oraziotti, M.; Neuburger, M.; Hamm, P.; Wenger, O.S. Intramolecular light-driven accumulation of reduction equivalents by proton-coupled electron transfer. *J. Am. Chem. Soc.* **2017**, *139*, 5225–5232. [[CrossRef](#)]
48. Aslan, J.M.; Boston, D.J.; MacDonnell, F.M. Photodriven multi-electron storage in disubstituted Ru<sup>II</sup> dppz analogues. *Chem.–Eur. J.* **2015**, *21*, 17314–17323. [[CrossRef](#)]
49. Lefebvre, J.F.; Schindler, J.; Traber, P.; Zhang, Y.; Kupfer, S.; Gräfe, S.; Baussanne, I.; Demeunynck, M.; Mouesca, J.M.; Gambarelli, S. An artificial photosynthetic system for photoaccumulation of two electrons on a fused dipyrrophenazine (dppz)–pyridoquinolinone ligand. *Chem. Sci.* **2018**, *9*, 4152–4159. [[CrossRef](#)]
50. Mills, I.N.; Porras, J.A.; Bernhard, S. Judicious design of cationic, cyclometalated Ir (III) complexes for photochemical energy conversion and optoelectronics. *Acc. Chem. Res.* **2018**, *51*, 352–364. [[CrossRef](#)]
51. Luo, Y.; Maloul, S.; Schönweiz, S.; Wächtler, M.; Streb, C.; Dietzek, B. Yield—not only lifetime—of the photoinduced charge-separated state in iridium complex–polyoxometalate dyads impact their hydrogen evolution reactivity. *Chem. Eur. J.* **2020**, *26*, 8045–8052. [[CrossRef](#)]
52. Luo, Y.; Maloul, S.; Endres, P.; Schönweiz, S.; Ritchie, C.; Wächtler, M.; Winter, A.; Schubert, U.S.; Streb, C.; Dietzek, B. Organic linkage controls the photophysical properties of covalent photosensitizer–polyoxometalate hydrogen evolution dyads. *Sustain. Energy Fuels* **2020**, *4*, 4688–4693. [[CrossRef](#)]
53. Shon, J.H.; Teets, T.S. Potent bis-cyclometalated iridium photoreductants with β-diketiminato ancillary ligands. *Inorg. Chem.* **2017**, *56*, 15295–15303. [[CrossRef](#)] [[PubMed](#)]
54. Shon, J.H.; Kim, D.; Rathnayake, M.D.; Sittel, S.; Weaver, J.; Teets, T.S. Photoredox catalysis on unactivated substrates with strongly reducing iridium photosensitizers. *Chem. Sci.* **2021**, *12*, 4069–4078. [[CrossRef](#)] [[PubMed](#)]
55. Shon, J.H.; Kim, D.; Gray, T.G.; Teets, T.S. β-Diketiminato-supported iridium photosensitizers with increased excited-state reducing power. *Inorg. Chem. Front.* **2021**, *8*, 3253–3265. [[CrossRef](#)]
56. Rohacova, J.; Ishitani, O. Rhenium (I) trinuclear rings as highly efficient redox photosensitizers for photocatalytic CO<sub>2</sub> reduction. *Chem. Sci.* **2016**, *7*, 6728–6739. [[CrossRef](#)]
57. Morimoto, T.; Ishitani, O. Modulation of the photophysical, photochemical, and electrochemical properties of Re (I) diimine complexes by interligand interactions. *Acc. Chem. Res.* **2017**, *50*, 2673–2683. [[CrossRef](#)]
58. Oppelt, K.; Mosberger, M.; Ruf, J.; Fernández-Terán, R.; Probst, B.; Alberto, R.; Hamm, P. Shedding light on the molecular surface assembly at the nanoscale level: Dynamics of a Re (I) carbonyl photosensitizer with a co-adsorbed cobalt tetrapyrrolyl water reduction catalyst on ZrO<sub>2</sub>. *J. Phys. Chem. C* **2020**, *124*, 12502–12511. [[CrossRef](#)]

59. Fernández-Terán, R.; Sévery, L. Living long and prosperous: Productive intraligand charge-transfer states from a rhenium (I) terpyridine photosensitizer with enhanced light absorption. *Inorg. Chem.* **2020**, *60*, 1334–1343. [[CrossRef](#)]
60. Wenger, O.S. A bright future for photosensitizers. *Nat. Chem.* **2020**, *12*, 323–324. [[CrossRef](#)]
61. Kobayashi, A.; Takizawa, S.Y.; Hirahara, M. Photofunctional molecular assembly for artificial photosynthesis: Beyond a simple dye sensitization strategy. *Coord. Chem. Rev.* **2022**, *467*, 214624. [[CrossRef](#)]
62. Wenger, O.S. Photoactive complexes with earth-abundant metals. *J. Am. Chem. Soc.* **2018**, *140*, 13522–13533. [[CrossRef](#)] [[PubMed](#)]
63. Socha, A.L.; Guerinot, M.L. Mn-euvering manganese: The role of transporter gene family members in manganese uptake and mobilization in plants. *Front. Plant. Sci.* **2014**, *5*, 106. [[CrossRef](#)] [[PubMed](#)]
64. Hou, H.J. Manganese-based materials inspired by photosynthesis for water-splitting. *Materials* **2011**, *4*, 1693–1704. [[CrossRef](#)]
65. Ye, S.; Ding, C.; Chen, R.; Fan, F.; Fu, P.; Yin, H.; Wang, X.; Wang, Z.; Du, P.; Li, C. Mimicking the key functions of photosystem II in artificial photosynthesis for photoelectrocatalytic water splitting. *J. Am. Chem. Soc.* **2018**, *140*, 3250–3256. [[CrossRef](#)]
66. Chen, C.; Chen, Y.; Yao, R.; Li, Y.; Zhang, C. Artificial Mn<sub>4</sub>Ca clusters with exchangeable solvent molecules mimicking the oxygen-evolving center in photosynthesis. *Angew. Chem. Int. Ed.* **2019**, *131*, 3979–3982. [[CrossRef](#)]
67. Herr, P.; Kerzig, C.; Larsen, C.B.; Häussinger, D.; Wenger, O.S. Manganese (I) complexes with metal-to-ligand charge transfer luminescence and photoreactivity. *Nat. Chem.* **2021**, *13*, 956–962. [[CrossRef](#)]
68. Wegeberg, C.; Wenger, O.S. Luminescent chromium (0) and manganese (i) complexes. *Dalton Trans.* **2022**, *51*, 1297–1302. [[CrossRef](#)]
69. Zhang, W.; Alonso-Mori, R.; Bergmann, U.; Bressler, C.; Chollet, M.; Galler, A.; Gawelda, W.; Hadt, R.G.; Hartsock, R.W.; Kroll, T. Tracking excited-state charge and spin dynamics in iron coordination complexes. *Nature* **2014**, *509*, 345–348. [[CrossRef](#)]
70. Auböck, G.; Chergui, M. Sub-50-fs photoinduced spin crossover in [Fe(bpy)<sub>3</sub>]<sup>2+</sup>. *Nat. Chem.* **2015**, *7*, 629–633. [[CrossRef](#)]
71. Jay, R.M.; Eckert, S.; Vaz da Cruz, V.; Fondell, M.; Mitzner, R.; Föhlisch, A. Covalency-driven preservation of local charge densities in a metal-to-ligand charge-transfer excited iron photosensitizer. *Angew. Chem. Int. Ed.* **2019**, *58*, 10742–10746. [[CrossRef](#)]
72. Huber-Gedert, M.; Nowakowski, M.; Kertmen, A.; Burkhardt, L.; Lindner, N.; Schoch, R.; Herbst-Irmer, R.; Neuba, A.; Schmitz, L.; Choi, T.K. Fundamental characterization, photophysics and photocatalysis of a base metal iron (II)-cobalt (III) dyad. *Chem. Eur. J.* **2021**, *27*, 9905–9918. [[CrossRef](#)] [[PubMed](#)]
73. Ghobadi, T.G.U.; Ghobadi, A.; Demirtas, M.; Buyuktemiz, M.; Ozvural, K.N.; Yildiz, E.A.; Erdem, E.; Yaglioglu, H.G.; Durgun, E.; Dede, Y. Building an iron chromophore incorporating prussian blue analogue for photoelectrochemical water oxidation. *Chem. Eur. J.* **2021**, *27*, 8966–8976. [[CrossRef](#)] [[PubMed](#)]
74. Jiang, T.; Bai, Y.; Zhang, P.; Han, Q.; Mitzi, D.B.; Therien, M. Electronic structure and photophysics of a supermolecular iron complex having a long MLCT-state lifetime and panchromatic absorption. *Proc. Natl. Acad. Sci. USA* **2020**, *117*, 20430–20437. [[CrossRef](#)] [[PubMed](#)]
75. Zobel, J.P.; Bokareva, O.S.; Zimmer, P.; Wölper, C.; Bauer, M.; González, L. Intersystem crossing and triplet dynamics in an iron(II) N-heterocyclic carbene photosensitizer. *Inorg. Chem.* **2020**, *59*, 14666–14678. [[CrossRef](#)] [[PubMed](#)]
76. Zimmer, P.; Müller, P.; Burkhardt, L.; Schepper, R.; Neuba, A.; Steube, J.; Dietrich, F.; Flörke, U.; Mangold, S.; Gerhards, M. N-heterocyclic carbene complexes of Iron as photosensitizers for light-induced water reduction. *Eur. J. Inorg. Chem.* **2017**, *2017*, 1504–1509. [[CrossRef](#)]
77. Duchanois, T.; Etienne, T.; Cebrián, C.; Liu, L.; Monari, A.; Beley, M.; Assfeld, X.; Haacke, S.; Gros, P.C. An iron-based photosensitizer with extended excited-state lifetime: Photophysical and photovoltaic properties. *Eur. J. Inorg. Chem.* **2015**, *2015*, 2469–2477. [[CrossRef](#)]
78. Zimmer, P.; Burkhardt, L.; Friedrich, A.; Steube, J.; Neuba, A.; Schepper, R.; Müller, P.; Flörke, U.; Huber, M.; Lochbrunner, S. The connection between NHC ligand count and photophysical properties in Fe(II) photosensitizers: An experimental study. *Inorg. Chem.* **2018**, *57*, 360–373. [[CrossRef](#)]
79. Kunnus, K.; Vacher, M.; Harlang, T.C.; Kjær, K.S.; Haldrup, K.; Biasin, E.; van Driel, T.B.; Pápai, M.; Chabera, P.; Liu, Y. Vibrational wavepacket dynamics in Fe carbene photosensitizer determined with femtosecond X-ray emission and scattering. *Nat. Commun.* **2020**, *11*, 634. [[CrossRef](#)]
80. Wehry, E.; Sundararajan, S. Intersystem crossing and internal conversion from the lowest charge-transfer singlet excited state of the (2, 9-dimethyl-1, 10-phenanthroline) copper (I) cation. *ChemComm* **1972**, *20*, 1135–1136.
81. Ahn, B.T.; McMillin, D.R. Studies of photoinduced electron transfer from bis (2,9-dimethyl-1, 10-phenanthroline) copper (I). *Inorg. Chem.* **1978**, *17*, 2253–2258. [[CrossRef](#)]
82. Phifer, C.C.; McMillin, D.R. The basis of aryl substituent effects on charge-transfer absorption intensities. *Inorg. Chem.* **1986**, *25*, 1329–1333. [[CrossRef](#)]
83. Eggleston, M.K.; Fanwick, P.E.; Pallenberg, A.J.; McMillin, D.R. A twist on the copper center in the crystal structure of [Cu(dnpp)<sub>2</sub>] PF<sub>6</sub> and the charge-transfer excited state?(dnpp= 2,9-Dineopentyl-1,10-phenanthroline). *Inorg. Chem.* **1997**, *36*, 4007–4010. [[CrossRef](#)]
84. Gandhi, B.A.; Green, O.; Burstyn, J.N. Facile oxidation-based synthesis of sterically encumbered four-coordinate bis (2, 9-di-tert-butyl-1,10-phenanthroline) copper (I) and related three-coordinate copper (I) complexes. *Inorg. Chem.* **2007**, *46*, 3816–3825. [[CrossRef](#)] [[PubMed](#)]

85. Sandroni, M.; Kayanuma, M.; Planchat, A.; Szuwarski, N.; Blart, E.; Pellegrin, Y.; Daniel, C.; Boujtita, M.; Odobel, F. First application of the HETPHEN concept to new heteroleptic bis (diimine) copper (I) complexes as sensitizers in dye sensitized solar cells. *Dalton Trans.* **2013**, *42*, 10818–10827. [[CrossRef](#)]
86. Housecroft, C.E.; Constable, E.C. The emergence of copper (I)-based dye sensitized solar cells. *Chem. Soc. Rev.* **2015**, *44*, 8386–8398. [[CrossRef](#)]
87. Kohler, L.; Hayes, D.; Hong, J.; Carter, T.J.; Shelby, M.L.; Fransted, K.A.; Chen, L.X.; Mulfort, K.L. Synthesis, structure, ultrafast kinetics, and light-induced dynamics of CuHETPHEN chromophores. *Dalton Trans.* **2016**, *45*, 9871–9883. [[CrossRef](#)]
88. Kohler, L.; Hadt, R.G.; Hayes, D.; Chen, L.X.; Mulfort, K.L. Synthesis, structure, and excited state kinetics of heteroleptic Cu (I) complexes with a new sterically demanding phenanthroline ligand. *Dalton Trans.* **2017**, *46*, 13088–13100. [[CrossRef](#)]
89. Zerk, T.J.; Bernhardt, P.V. Redox-coupled structural changes in copper chemistry: Implications for atom transfer catalysis. *Coord. Chem. Rev.* **2018**, *375*, 173–190. [[CrossRef](#)]
90. Levi, G.; Biasin, E.; Dohn, A.O.; Jónsson, H. On the interplay of solvent and conformational effects in simulated excited-state dynamics of a copper phenanthroline photosensitizer. *Phys. Chem. Chem. Phys.* **2020**, *22*, 748–757. [[CrossRef](#)]
91. Zhang, Y.; Zedler, L.; Karnahl, M.; Dietzek, B. Excited-state dynamics of heteroleptic copper (I) photosensitizers and their electrochemically reduced forms containing a dipyrroline moiety—a spectroelectrochemical transient absorption study. *Phys. Chem. Chem. Phys.* **2019**, *21*, 10716–10725. [[CrossRef](#)]
92. Velasco, L.; Llanos, L.; Levín, P.; Vega, A.; Yu, J.; Zhang, X.; Lemus, L.; Aravena, D.; Moonshiram, D. Structure and excited-state dynamics of dimeric copper (I) photosensitizers investigated by time-resolved X-ray and optical transient absorption spectroscopy. *Phys. Chem. Chem. Phys.* **2021**, *23*, 3656–3667. [[CrossRef](#)] [[PubMed](#)]
93. Mara, M.W.; Fransted, K.A.; Chen, L.X. Interplays of excited state structures and dynamics in copper (I) diimine complexes: Implications and perspectives. *Coord. Chem. Rev.* **2015**, *282*, 2–18. [[CrossRef](#)]
94. Stroschio, G.D.; Ribson, R.D.; Hadt, R.G. Quantifying entatic states in photophysical processes: Applications to copper photosensitizers. *Inorg. Chem.* **2019**, *58*, 16800–16817. [[CrossRef](#)] [[PubMed](#)]
95. Rosko, M.C.; Wells, K.A.; Hauke, C.E.; Castellano, F.N. Next generation cuprous phenanthroline MLCT photosensitizer featuring cyclohexyl substituents. *Inorg. Chem.* **2021**, *60*, 8394–8403. [[CrossRef](#)]
96. Garakyaraghi, S.; McCusker, C.E.; Khan, S.; Koutnik, P.; Bui, A.T.; Castellano, F.N. Enhancing the visible-light absorption and excited-state properties of Cu(I) MLCT excited states. *Inorg. Chem.* **2018**, *57*, 2296–2307. [[CrossRef](#)]
97. Takeda, H.; Kamiyama, H.; Okamoto, K.; Irimajiri, M.; Mizutani, T.; Koike, K.; Sekine, A.; Ishitani, O. Highly efficient and robust photocatalytic systems for CO<sub>2</sub> reduction consisting of a Cu (I) photosensitizer and Mn(I) catalysts. *J. Am. Chem. Soc.* **2018**, *140*, 17241–17254. [[CrossRef](#)]
98. Kim, J.; Whang, D.R.; Park, S.Y. Designing highly efficient Cu<sup>I</sup> photosensitizers for photocatalytic H<sub>2</sub> evolution from water. *ChemSusChem* **2017**, *10*, 1883–1886. [[CrossRef](#)]
99. Heberle, M.; Tschierlei, S.; Rockstroh, N.; Ringenberg, M.; Frey, W.; Junge, H.; Beller, M.; Lochbrunner, S.; Karnahl, M. Heteroleptic Copper Photosensitizers: Why an extended  $\pi$ -system does not automatically lead to enhanced hydrogen production. *Chem. Eur. J.* **2017**, *23*, 312–319. [[CrossRef](#)]
100. Giereth, R.; Frey, W.; Junge, H.; Tschierlei, S.; Karnahl, M. Copper photosensitizers containing P<sup>^</sup>N ligands and their influence on photoactivity and stability. *Chem. Eur. J.* **2017**, *23*, 17432–17437. [[CrossRef](#)]
101. Takeda, H.; Ohashi, K.; Sekine, A.; Ishitani, O. Photocatalytic CO<sub>2</sub> reduction using Cu(I) photosensitizers with a Fe(II) catalyst. *J. Am. Chem. Soc.* **2016**, *138*, 4354–4357. [[CrossRef](#)]
102. Zhang, Y.; Heberle, M.; Wächtler, M.; Karnahl, M.; Dietzek, B. Determination of side products in the photocatalytic generation of hydrogen with copper photosensitizers by resonance Raman spectroelectrochemistry. *RSC Adv.* **2016**, *6*, 105801–105805. [[CrossRef](#)]
103. Takeda, H.; Monma, Y.; Sugiyama, H.; Uekusa, H.; Ishitani, O. Development of visible-light driven Cu (I) complex photosensitizers for photocatalytic CO<sub>2</sub> reduction. *Front. Chem.* **2019**, *7*, 418. [[CrossRef](#)] [[PubMed](#)]
104. Giereth, R.; Reim, I.; Frey, W.; Junge, H.; Tschierlei, S.; Karnahl, M. Remarkably long-lived excited states of copper photosensitizers containing an extended  $\pi$ -system based on an anthracene moiety. *Sustain. Energy Fuels* **2019**, *3*, 692–700. [[CrossRef](#)]
105. Müller, C.; Schulz, M.; Obst, M.; Zedler, L.; Gräfe, S.; Kupfer, S.; Dietzek, B. Role of MLCT States in the Franck–Condon Region of Neutral, Heteroleptic Cu (I)–4 H-imidazolate Complexes: A Spectroscopic and Theoretical Study. *J. Phys. Chem. A* **2020**, *124*, 6607–6616. [[CrossRef](#)]
106. Pann, J.; Roithmeyer, H.; Viertl, W.; Pehn, R.; Bendig, M.; Dutzler, J.; Kriesche, B.; Brüggeller, P. Phosphines in artificial photosynthesis: Considering different aspects such as chromophores, water reduction catalysts (WRCs), water oxidation catalysts (WOCs), and dyads. *Sustain. Energy Fuels* **2019**, *3*, 2926–2953. [[CrossRef](#)]
107. Zhang, Y.; Ren, K.; Wang, L.; Wang, L.; Fan, Z. Porphyrin-based heterogeneous photocatalysts for solar energy conversion. *Chin. Chem. Lett.* **2021**, *33*, 33–60. [[CrossRef](#)]
108. Al Mogren, M.M.; Ahmed, N.M.; Hasanein, A.A. Molecular modeling and photovoltaic applications of porphyrin-based dyes: A review. *J. Saudi Chem. Soc.* **2020**, *24*, 303–320. [[CrossRef](#)]
109. Ramasamy, S.; Bhagavathichari, M.; Suthanthiraraj, S.A.; Pichai, M. Mini review on the molecular engineering of photosensitizer: Current status and prospects of metal-free/porphyrin frameworks at the interface of dye-sensitized solar cells. *Dyes Pigm.* **2022**, *203*, 110380. [[CrossRef](#)]

110. Zarrabi, N.; Poddutoori, P.K. Aluminum (III) porphyrin: A unique building block for artificial photosynthetic systems. *Coord. Chem. Rev.* **2021**, *429*, 213561. [[CrossRef](#)]
111. Giannoudis, E.; Benazzi, E.; Karlsson, J.; Copley, G.; Panagiotakis, S.; Landrou, G.; Angaridis, P.; Nikolaou, V.; Matthaiaki, C.; Charalambidis, G. Photosensitizers for H<sub>2</sub> evolution based on charged or neutral Zn and Sn porphyrins. *Inorg. Chem.* **2020**, *59*, 1611–1621. [[CrossRef](#)]
112. Luo, G.F.; Biniuri, Y.; Chen, W.H.; Wang, J.; Neumann, E.; Marjault, H.B.; Nechushtai, R.; Winkler, M.; Happe, T.; Willner, I. Modelling photosynthesis with Zn<sup>II</sup>-protoporphyrin all-DNA G-quadruplex/apramer scaffolds. *Angew. Chem. Int. Ed.* **2020**, *132*, 9248–9255. [[CrossRef](#)]
113. Kunnus, K.; Li, L.; Titus, C.J.; Lee, S.J.; Reinhard, M.E.; Koroidov, S.; Kjær, K.S.; Hong, K.; Ledbetter, K.; Doriese, W.B. Chemical control of competing electron transfer pathways in iron tetracyano-polypyridyl photosensitizers. *Chem. Sci.* **2020**, *11*, 4360–4373. [[CrossRef](#)] [[PubMed](#)]